NOTE TO USERS

3D Characterization of the Hemodynamic Parameters in a Stented Coronary Artery

Isam Faik

McGill University, Montreal

February, 2005

A thesis submitted to McGill University in partial fulfillment of the requirements of the degree of Masters of Engineering

Your file Votre référence
ISBN: 0-494-12600-0
Our file Notre référence
ISBN: 0-494-12600-0

To my parents

To Sarah

To everyone with a stent in his/her heart

Acknowledgments

All praise is due to God, the most gracious, the most merciful.

I first and foremost would like to acknowledge the support, advice, and gentleness of my supervisor, Dr. Rosaire Mongrain, throughout my master's degree. I also thank my co-supervisor Dr. Olivier Bertrand as well as the Montreal Hear Institute (Montreal) and Laval Hospital (Quebec city) for their support towards the accomplishment of this work.

I would like to extend special thanks to my parents, for simply being my parents, and for all their help, support, and prayers from my first day in this world to the day I submit this thesis. I also thank my wife Sarah, who became my wife at the most critical time of this work, for her tireless encouragement, her patience and her continuous smile. I would also like to thank my colleagues Youssef, Bilal, Tin, Neil, Adrian, Akshay, and Jean for their assistance and friendship.

.

Abstract

Stenting is becoming the major interventional cardiology procedure worldwide. However restenosis remains a major limitation to the effectiveness of stents. Alterations to the local hemodynamics in the stented segment of the artery is a potential factor in the development of in-stent restenosis. The characterization of wall shear stress and of blood flow patterns in a stented artery is therefore necessary for a good understanding of the phenomenon. We have used a time-dependent 3D numerical model of a stented coronary artery to study the characteristics of the blood flow and the shear stress distribution. Our results show that the presence of the stent results in significant secondary flow. Regions of low shear stress were localized around the struts while the struts exhibited high values of shear stress. These results support the hypothesis that local hemodynamics may affect the development of in-stent restenosis and can guide the choice of stent geometries for future stent designs.

Résumé

L'utilisation de stent (ou tuteur coronarien) est en train de devenir la principale procédure en cardiologie interventionelle partout dans le monde. Cependant, la resténose reste toujours une limitation importante à l' efficacité des stents. Les modifications à l' hémodynamique dans les régions stentées de l'artère constituent un élément potentiel du développement de la resténose intrastent. La caractérisation du cisaillement et des profils de l'écoulement du sang dans les artères stentées est donc nécessaire pour atteindre une bonne compréhension de ce phénomène. Nous avons développé un modèle transitoire et tri-dimensionel d'un artère coronaire pour étudier les caractéristiques de l'écoulement du sang et de la distribution du cisaillement. Nos résultats démontrent que la présence du stent produit des écoulements secondaires importants. Les régions qui présentent des valeurs basses de cisaillement ont été localisées autour des filaments alors que les bouts des filaments sont soumis à des valeurs élevées de cisaillement. Ces résultats appuient l'hypotèse que l' hémodynamique locale peut affecter le développement de la resténose intrastent et peut guider le choix de la géométrie du stent pour les modèles futurs.

Table of Contents

List of figures

List of Tables

Chapter 1: Introduction

In the 2004 World Health Report of the World Health Organization (WHO), cardiovascular diseases (CVD) are stated to be the cause of 16.7 million deaths worldwide, making them the leading cause of mortality in the industrialized world and in a number of developing countries. Atherosclerosis, or the buildup of plaque in the inner lining of the artery wall, is the most common form of CVD. When atherosclerosis develops in the blood vessels that supply the heart muscle with oxygen and nutrients, called coronary arteries, it can result in a severe narrowing of the artery and eventually lead to a heart attack.

Stenting is an interventional cardiology procedure that led to significant advancements in the treatment of atherosclerosis. Stents are wire mesh tubular structures that are deployed from the tip of a catheter against the arterial wall to improve the patency of the affected artery and restore blood flow through the stenosed region. However, in-stent restenosis (ISR) remains a major limitation to the success rate of stent implantation. The mechanisms responsible for ISR are not yet fully understood, however, there is an important body of evidence that alterations in the hemodynamics of the stented region are an important factor in ISR pathogenesis.

Stent expansion against the artery wall causes injury to the endothelium, a single layer of cells lining the inner surface of the artery. Endothelial cells regrowth is necessary for a proper healing of the treated artery. Furthermore, the denudation of the

endothelium, along with the presence of a metallic surface, lead to platelet aggregation that results in the formation of a thrombus layer that correlates with the incidence and severity of restenosis. Both reactions, endothelial cell regrowth and platelet adhesion, are affected by the local hemodynamics.

Previous studies have used computational fluid dynamics (CFD) to investigate the alterations to blood flow patterns and wall shear stress (WSS) introduced by the presence of a stent. Two-dimensional (2D) and three-dimensional (3D) models of different stent types were used to obtain a localized characterization of these hemodynamic parameters within the stented region. However, given the high computational cost of these simulations, only 2D models incorporated the effect of blood pulsation, while 3D simulations were based on steady flow conditions. In this study, we developed a 3D model of an experimental stent to obtain one of the first descriptions of the intricacies of blood flow in the stented segment of a coronary artery that combines both the three dimensional features of the flow and blood pulsation. Through this realistic model we are able to obtain both the spatial and temporal changes in blood velocity and WSS in the inter-strut zones and hence gain a better understanding of the mechanisms through which they eventually affect the development of restenosis.

Chapter 2: Medical Context

1. Arteries Anatomy

Arteries are vessels that convey blood from the heart to other organs in the body. The arteries are composed of three layers: an internal or endothelial layer (*tunica intima*); a middle or muscular layer (*tunica media*); and an external or connective-tissue layer (*tunica adventitia*). However, the proportion and structure of each layer varies with the size and function of the particular artery.

The intima is a fine, transparent, colorless structure, which is highly elastic. It consists of an inner monolayer of endothelial cells lining the lumen and is bound on the outside by internal elastic lamina, a fenestrated sheet of elastin fibers having principally a longitudinal direction. The thin subendothelial space in between contains thin elastin and collagen fibers along with a few smooth muscle cells (SMCs).

The media is distinguished from the intima by its color and by the transverse arrangement of its fibers. It consists principally of plain muscle fibers in fine bundles, arranged in lamellæ and disposed circularly around the vessel. It is to this layer that the thickness of the wall of the artery is mainly due.

The adventitia consists mainly of fine and closely felted bundles of white connective tissue, but also contains elastic fibers.

Like other organs of the body, arteries are supplied with blood through other vessels. These nutrient vessels, called the vasa vasorum, arise from a branch of the artery, or from a neighboring vessel, at some considerable distance from the point at which they are distributed.

Coronary Arteries:

The coronary arteries are the vessels that carry blood to the heart muscle. Because the heart muscle is continuously working (as opposed to other muscles of the body, which are often at rest), it has a very high requirement for oxygenated blood. The coronary arteries are vitally important for supplying that blood, and allowing the heart to work normally. Two major coronary arteries arise from the aorta – the right coronary artery (RCA) and the left main artery (LM). The left main artery quickly branches into two large arteries – the left anterior descending artery (LAD) and the circumflex artery (Cx). These arteries, when healthy, are capable of autoregulation to maintain coronary blood flow at levels appropriate to the needs of the heart muscle (*myocardium*).

The coronary arteries are classified as "end circulation", since they represent the only source of blood supply to the myocardium: there is no redundant blood supply, which is why blockage of these vessels can be critical.

2. Atherosclerosis

Atherosclerosis is the leading cause of death in the industrialized world and a number of developing countries, and estimates have been given, that at its present rate of growth, it will be the major cause of death by the year 2020 in the entire world [1, 2].

Atherosclerosis is the process in which deposits of fatty substances, cholesterol, cellular waste products, calcium and other substances build up in the inner lining of

an artery. This buildup is called atherosclerotic plaque and usually affects large and medium-sized arteries.

The process starts as an adaptive response to insults to the endothelium and smooth muscle cells of the wall of the artery, and progresses to the formation of atherosclerotic plaques which narrow and may totally obstruct the lumen of the affected artery [3]. However, most of the damage occurs when these plaques become fragile and rupture or ulcerate. In this case, exposed contents cause platelets (thrombocytes) to adhere and aggregate creating a thrombus over the site of the plaque. If this happens and blocks a coronary artery, it causes a heart attack. If it blocks a blood vessel that feeds the brain, it causes a stroke. And if blood supply to the arms or legs is reduced, it can cause difficulty walking and eventually gangrene.

Risk factors for atherosclerosis are numerous and are not all well known. Clearly, hypercholestrolemia is a dominant risk factor for the disease [1, 4, 5]. Diabetes, hypertension, glucose intolerance, physical inactivity, cigarette smoking, obesity, family history, hypercoagulability...etc are all factors that increase the chances of the development of atherosclerotic plaques [6-8]. However, more recently, accumulating evidence suggests that atherosclerosis is also an inflammatory disease, meaning that infections could play an important role in its etiology [3].

Throughout history, different theories were postulated for the pathogenesis of atherosclerosis [9]. The encrustation theory by Rokitansky suggested that atherosclerosis begins in the intima with deposition of thrombus and its subsequent organization by infiltration of fibroblasts and secondary lipid deposition. The lipid theory by Virchow suggested that atherosclerosis starts with the lipid transudation into the arterial wall leading to intimal proliferation. More recently, the response-to-

endothelial injury theory by Ross linked the beginning of atherosclerosis to endothelial injury, which makes the artery susceptible to accumulation of lipids and deposition of thrombus. The response-to-vascular injury is currently the most accepted theory, and it postulates that injury to the endothelium by local disturbances of blood flow along with systemic risk factors perpetuates a series of events that culminate in development of atherosclerotic plaque [10].

Role of the Endothelium

The endothelium is the innermost layer of cells that lines the blood vessels. Until quite recently the endothelium was thought to be an inert lining of the blood vessels but it is now becoming clear that endothelial cells play a number of essential and complex roles within the body.

These roles include: 1- a selective barrier to the passage of molecules and cells between the blood and the surrounding bodily tissue; 2- a nonthrombogenic interface between the blood and the artery; 3- Modulation of vasodilation and vasoconstriction by the release of small molecules (prostacyclin PGI2, endothelin ET); 4- formation and secretion of growth-regulatory molecules and cytokines; 5- summoning and capturing white blood cells (leukocytes) to the site of an infection; 6- nonadherent surface for leukocytes; 7- modifying (oxidizing) lipoproteins as they are transported into the artery wall [11].

Any disruption or alteration to these roles can be the first sign of endothelial dysfunction (ED) which leads to the following changes in endothelial function:

Increased permeability to lipoproteins, decreased nitric oxide production, increased leukocyte migration and adhesion, prothrombotic dominance, vascular growth stimulation, vasoactive substance release [11].

3. Atherosclerosis Treatment: Angioplasty

The treatment of atherosclerosis is focused on the revascularisation of the obstructed arteries to ensure sufficient blood supply to the myocardium. Therefore, depending on the severity of the occlusion and on the combination of future risks, one of the following treatments is used: Pharmacotherapy, Coronary Artery Bypass Grafting (CABG), or Percutaneous Transluminal Coronary Angioplasty (PTCA)[1].

The main objective in using drugs for the treatment of atherosclerosis is the control of risk factors associated with the disease [12]. Mechanisms of action include the reduction of the level of low-density lipids (Statin drugs), the modulation of the proliferation of smooth muscle cells (ACE inhibitors), the prevention of thrombus formation (Aspirin), the protection against vascular lesion (Calcium antagonist), and the reduction of platelet aggregation and blood viscosity (n-3 fatty acids) [13, 14].

CABG is an open-heart surgical placement of a blood vessel (vein or artery), called a graft, taken from the arm, leg, or chest, to bypass a blockage in the coronary artery. There are two main types of CABG operations, one that uses an extracorporeal

[1] "Percutaneous" means that access to the blood vessel is made through the skin, and "Transluminal" means that the procedure is performed within the blood vessel

pump to maintain blood perfusion to the body while the heart is stopped throughout the surgery and another one that uses retraction and stabilizing devices that expose the coronary artery, allowing the performance of the operation, while the heart continues to beat [15].

PTCA was introduced by Gruentzig in 1977 [16]. In a PTCA operation, a catheter with a special balloon on its tip is carefully threaded into the occluded artery. The Balloon is then inflated to stretch open the narrowed area of the lumen, hence improving its patency. The major mechanisms of luminal enlargement in PTCA include medial dissection, intimal desquamation, intimal and medial disruption in the arterial wall located opposite the plaque, release of plaque content into the lumen, and the stretching of the vessel circumference [17].

Both Angioplasty and bypass grafting have shown remarkable success in the revascularization of coronary arteries. However, all randomized trials comparing the two modalities have shown that they are equivalent in terms of survival, infarct free survival, or future neurological complications [18-20]. The choice of one procedure over the other is then made depending on a number of patient specific factors including the lesion morphology, the number of blocked arteries, the severity of the blockages, the location of the blockages, other medical conditions, and surgical risk [20]. PTCA has the advantages of being performed with local anesthesia, having a shorter recovery time, and simply the advantage of not being a surgery. However, the need for repeat operations is still higher after PTCA compared to CABG, although current advances in PTCA are promising for a substantial reduction in its rate.

4. Restenosis

As mentioned in the previous section, the major limitation to coronary angioplasty remains the need for repeat revascularization at a high rate. The main cause of this need is restenosis.

Restenosis is defined as the re-narrowing of the treated segment, which reaches or exceeds 50% of the lumen in the adjacent normal segment of the artery. Several studies have reported a restenosis rate that ranges from 30% to 40% of the cases treated by balloon dilation [21-23].

Restenosis is different from native atherosclerosis in its nature and its development. Several distinct processes are involved in the pathogenesis of restenosis: vessel recoil, neointimal formation, constrictive vascular remodeling, matrix formation, and early thrombus formation [24]. Vessel recoil is due to the elastic properties of the arterial wall and occurs in the first 60 minutes after balloon dilation. Neointimal formation, also called neointimal hyperplasia, is a vascular repair process that takes place through the proliferation and migration of the smooth muscle cells and an increase in extracellular matrices. Vascular remodeling is the lasting structural changes in the vessel wall in response to hemodynamic stimuli or vessel injury. It is associated with a redistribution of the extracellular matrix and smooth muscle cells in the media and the adventitia. Different studies have shown vascular remodeling to account for three quarters of lumen loss following balloon angioplasty.

Different factors affect the possibility of restenosis development after an angioplasty procedure. These factors include: the severity and location of the athorosclerotic

lesion, the morphology of the plaque, and the size of the treated artery [25]. For example, restenosis seems to be more frequent after the treatment of long lesions, making the length of the original stenosis a strong predictor of future re-narrowing [26]. The minimal diameter in the stenosed artery has also been shown to negatively correlate with the rate of restenosis [27]. Other factors are more related to the operation itself. For example, the minimal lumen diameter after an angioplasty procedure is associated with higher rate of restenosis. This means that a larger lumen diameter after the operation is better for the prevention of restenosis [28]. Other factors are more patient dependent. The presence of diabetes, for instance, is considered an important predictor of restenosis [29].

5. Restenosis Treatment: Stents

Given the significant limitation that restenosis imposes on the efficacy of coronary angioplasty, different therapies were developed or are being tested to try to reduce its rate to the lowest possible level. These therapies include systemic delivery of drugs, gene therapy, atherectomy, cutting balloon angioplasty, laser angioplasty, and endovascular stenting.

The drugs that are delivered systemically are, in general, chosen for their antiplatelet, antithrombotic, antiproliferative, or anti-inflammatory effect. However, the need for high doses and high delivery time, which entails a risk of systemic toxicity, limits the use of many of these drugs [30, 31]. In addition, systemically delivered drugs are not able to counter recoil which accounts for most of lumen loss after balloon angioplasty.

The principle in atherectomy is to physically remove the plaque instead of simply displacing it as it is done in balloon angioplasty. Several types of atherectomy devices are used including directional, transluminal excisional, rotational, and laser atherectomy. Rotational atherectomy, for example, uses rotating burrs to remove the plaque by ablation, causing it to disperse into the blood flow. It is mainly used for heavily calcified or fibrotic lesions that are difficult to access by angioplasty [32]. It is often used in combination with angioplasty.

The most common form of treatment to reduce restenosis after balloon angioplasty is endovascular stenting. Stents are wire mesh tubes that are placed on the site of angioplasty. Stents prevent restenosis by providing scaffolding to the artery wall against recoil, by achieving a larger lumen diameter hence reducing neointimal hyperplasia, and by preventing vascular remodeling [33]. The use of stents with coronary interventions has increased from 10% in 1994 to over 90% in 2002 [34].

There are over 100 stent designs that are currently being used worldwide, and more are being evaluated [35]. Different designs employ different materials, different fabrication methods, and different geometries. There are two major categories of stents: balloon-expandable and self-expanding. Balloon-expandable stents are manufactured and mounted on the balloon in their collapsed configuration, while self-expanding stents are manufactured in their expanded shape and then compressed and constrained in a delivery system.

The material used for stent manufacturing has to satisfy a number of criteria including corrosion resistance, biocompatibility and radiopacity. Balloon-expandable stents plastically deform to their expanded shape, so the ideal material for them is

one with low yield stress and high elastic modulus to minimize recoil. Stainless steel 316L is the standard material for these stents. Alternative materials include tantalum, platinum alloys, cobalt alloys, and niobium alloys. For self-expanding stents, the material should exhibit large elastic strains. Nitinol is a nickel-titanium alloy and it is the most widely used material for this category of stents [36].

Different factors determine the geometry chosen for a particular stent, the major one being the attempt to find an optimal balance between strength and flexibility. The effect of geometry on hemodynamic parameters is another important factor in the choice of a particular geometry. There are different ways to categorize the existing stent geometries. One way is to differentiate between open-cell and closed-cell constructions. We can also distinguish between stents made with successive sinusoidal, S-, U-, V-, or N-shaped patterns.

The base material from which stents are manufactured can be in the form of a tube, wire, or sheet metal. Tube-based stents are manufactured using laser cutting and constitute the vast majority of existing stents while wire-based stents are manufactured using coiling, knitting, and braiding. Other manufacturing methods include water jet cutting and photochemical etching.

6. In-stent Restenosis (ISR)

Despite the significant reduction in restenosis rates with the use of stents, in-stent restenosis remains a significant limitation to the efficacy of stents for the treatment of atherosclerosis. Many groups have conducted randomized trials and have

reported restenosis rates of over 20% for patients treated with coronary stents [21, 22, 37].

The pathogenesis of ISR is different from that of restenosis after balloon angioplasty. First, because, by their scaffolding effect, stents prevent acute vascular recoil following procedure. In addition, many studies have shown that while lumen renarrowing after balloon angioplasty is due to both neointimal formation and vascular remodeling, restenosis after stenting is mainly due to neointimal hyperplasia [38-40]. Some studies however have established a correlation between peri-stent remodeling and lumen loss due to intra-stent intimal proliferation [41].

A number of methods have been developed to reduce the rate of ISR and improve the effectiveness of stent implantation. The most common technique developed to prevent ISR is the use of drug eluting stents (DES). DES first clinical results have been very promising but the procedure is still novel to be able to make definitive statements about its rate of success. Another method used to prevent ISR is the use of compliance matching stents (CMS) [42]. In a CMS, the distal and proximal ends of the stent are modified to reduce the compliance mismatch between the stented segment of the artery and the rest of the artery. This compliance mismathch has been correlated with the development of ISR. A new method that is being tested at the same center where Plamaz patented the world's first stent (Health Science Center, University of Texas), is to use photo etching to engrave grooves into the stent. The rational behind this method is that endothelial cells have been shown to more readily migrate to grooved stent struts. This migration is expected to reduce the chance of developing ISR. Another way to improve the clinical outcome of stents is simply by

developing stent designs that take the local hemodynamics into consideration and affect the blood flow patterns in a way that would inhibit neointimal hyperplasia.

Chapter 3: Literature Review

Many studies have established a strong correlation between alterations to the hemodynamic parameters in different sites of the vascular system and the early development of native atherosclerosis. These sites include the aortic bifurcation [43], the common carotid artery [44], the carotid bifurcation [45], and the abdominal aorta [46]. He and Ku conducted similar research on the coronary arteries and found a strong correlation between the distribution of low and oscillatory wall shear stress and the locations of atherosclerosis development [47].

In the other hand, to establish a correlation between changes in hemodynamic parameters and the occurrence of ISR requires that we single out the biomechanical factors from other factors involved in the pathogenesis of the disease. A first step towards setting up the correlation is to show a consistent effect of stent design on the development of ISR.

A number of studies have compared different stent designs in similar conditions and concluded that neointimal proliferation is significantly affected by stent design [48-50]. Kastrati et al (2001) have conducted a study with 4,510 patients and showed that after vessel size, stent design is the second most important factor in determining the hyperplastic response of the vessel wall [51]. However, this effect can be due to a number of post deployment parameters. For instance, stent geometry can influence vascular strain which may affect cellular orientation and enhance cell proliferation [52]. Stent design can also affect arterial injury after deployment. In fact, Schwartz et

al(1992) have shown an effect of vascular injury on neointimal proliferation [53]. However, Garasic et al (2000) have shown that stent geometry determine intimal thickening independent of injury [54]. In the other hand, stent-imposed alterations to the hemodynamics in the lesion area have been presented by many goups as the most viable design-related cause of neointimal proliferation [55-57].

This apparent relationship between blood flow parameters and neointimal proliferation has prompted many groups to study blood flow patterns after stent implantation to better understand the mechanism by which they eventually lead to the development of ISR. The characterization of these flow patterns has been attempted in many studies using in-vivo, ex-vivo, and in-vitro experiments, as well as numerical simulations based on CFD.

LaDisa et al (2002) conducted in-vivo experiments to study the effect of stent implantation on the alterations to coronary hemodynamics in dogs [58]. They used different transducers and micromanometers to measure different hemodynamic parameters. Other parameters such as shear stress were calculated from the measured values and plotted as functions of time. However, these experiments only allow for the measurement and calculation of values at particular points and do not provide information about the distribution of these parameters. Their results show an increase in coronary blood flow and wall shear stress after stent implantation in a healthy vessel.

Berry et al (1997) conducted in-vitro experiments on two stent models under physiologic pulsatile flow conditions [59]. Their results revealed flow stagnation between stent struts during systole and large-scale vortex formation during diastole.

In another in-vitro study Benard et al (2003) used particle image velocimetry (PIV) to study blood flow through a stented section under steady state conditions [60]. Using this flow visualization technique, they were able to measure the velocity field in the inter-strut zones for a flat model of the stent. They found that the highest values of shear stress in the blood were close to the stent struts. They were also able to see a slight recirculation zone between struts that were close to each other with a development of the eddy as the flow rate was increased.

In the other hand, computational fluid dynamics has been used by a number of research groups to study the flow patterns in a stented artery. Henry (2000) used the finite volume method to solve the governing equations for the blood flow in a 2D axisymmetric stent model with a physiologic flow waveform at the inlet boundary [61]. He also modeled the solid mechanics of the arterial wall (but not coupled with CFD) and found the arteries stiffness to be significantly higher for a stented artery. This allowed him to assume a rigid wall boundary condition for the CFD model. His CFD results showed the stent struts spacing to be the most important parameter affecting flow patterns. Berry et al. (2000) generated a 2D model of the near wall area of a braided stent [62]. They modeled the crossover point of the wire mesh, and hence represented the stent by a sequence of two overlapping struts. They studied the effect of certain stent design parameters such as wire spacing and wire diameter on the flow patterns in the stented region for two different vessel diameters and for two flow conditions (resting and exercise). Their results show the formation of stagnation zones between the stent struts. These zones were either continuous from one wire to the next or detached with the formation of two vortices depending on the different combinations of the aforementioned parameters.

Schachter and Barakat (2001) also used 2D models to investigate the effect of certain stent parameters on the blood flow dynamics in the stented region and downstream of the stent [63]. They applied a non-reversing sinusoidal waveform with a frequency of 1Hz as an idealization of the blood flow pulsatility. They have also created 3D models with steady flow conditions of stents placed within curved arterial segments. They also used the finite volume method based on the commercial software FLUENT to solve the governing equations. Their results show that the size of the flow separation zone is not affected by the number of stent struts, especially when this number is higher than three. They also showed that while the size of the flow separation zone increases with increasing Reynolds' number and strut thickness, which is an expected result, the separation zone periodically appeared and disappeared when the simulation involved pulsatile flow. They also showed that inter-strut spacing affect the lenght of the separation zone but only until a threshold value after which this length becomes insensitive to inter-strut spacing. Their 3D simulations reveal that the vessel curvature leads to considerable skewness in the flow velocity profile.

LaDisa et al (2003) created 3D models of the Palmaz-Schatz stent in geometries of canine coronary arteries constructed based on in vivo data and subject to steady flow representing the minimum and maximum coronary flow velocities [64]. They compared their results with simulations on models of unstented arteries and found that the presence of the stent resulted in noticeable out-of-plane velocity components. They presented a 3D distribution of the wall shear stress in the stented region using a colour map. These distributions showed the shear stress to be highest on the struts and exhibited a slight decrease with each subsequent stent. They also

show areas of low shear stress to be larger when struts are orthogonal to the blood flow. The values of minimum shear stress in the stented region were also shown to increase (30%) for the minimum velocity boundary condition and to decrease (13%) for maximum velocity boundary condition.

Only recently, the first study of the stent hemodynamics that uses time-dependent 3D models have been published by LaDisa et al (2005) [65]. In this study they developed 3D models of canine coronary arteries with a Palmaz-Schatz stent and applied the physiological blood velocity waveform at the canine LAD coronary artery. Their results show that pronounced stagnation regions develop right before flow deceleration at the maxima of the flow waveform. They also compared time-dependent simulations with the ones that impose steady-state velocity and found that the steady-state assumption results in an underestimation of the distribution of wall shear stress during flow acceleration and an overestimation of this distribution during flow deceleration.

Chapter 4: Blood Flow Biomechanics

1. Governing Equations

The basic transport equations that govern blood flow are the mathematical representation of the conservation principles that include the conservation of mass and the conservation of momentum. Hence, blood flow in the artery has to satisfy both the continuity equation and the Navier-Stokes equation.

Blood is considered a homogeneous and incompressible fluid. Therefore, the continuity equation is reduced to:

$$\nabla . u = 0 \tag{1}$$

Where u is the local velocity vector in mm/s

Or in tensor form:

$$u_{j,j} = 0 \tag{2}$$

After the application of certain assumptions and simplification, the Navier-Stokes equation for blood flow in an artery is given by:

$$\rho(\frac{\partial u}{\partial t} + u.\nabla u) = -\nabla p + \mu \nabla^2 u \tag{3}$$

where p is the local pressure in Pa, ρ is blood density in $\frac{g}{cm^3}$, μ is blood viscosity in Pa.s = $10.\frac{g}{cm \cdot s}$ = 1 Poiseuille = 10 Poise.

Or in tensor form:

$$\rho\left(\frac{\partial u_i}{\partial t} + u_j u_{i,j}\right) = -p_i + \mu\left[u_{i,j}\right]_{,j} \tag{4}$$

These assumptions include considering blood flow to be laminar throughout the area of interest and assuming the blood to possess Newtonian rheological properties (i.e. to be a fluid in which shear stress is directly proportional to shear rate). The latter assumption is deemed valid since, at shear rates higher than 100 s^{-1}, blood behaves largely as a Newtonian fluid [66], and coronary arteries, in general, experience wall shear rates that are higher than this value.

In addition, vessel wall compliance is neglected and the artery is regarded as a rigid wall to avoid the need for structural equations that would have to be coupled with the above two fluid equations. This assumption is supported by the study of Berry et al (2000) [62] in which they observed the change in diameter in the stented segment to be much smaller than that of the regions distal and proximal to the stent. In their study, the stent region exhibited an average diameter change of less than 2%.

2. Blood Properties

Blood consists of a suspension of different corpuscles such as the red blood cells (erythrocytes), the white blood cells (leucocytes), and the platelets (thrombocytes), in a Newtonian liquid called plasma or liquor sanguinis. Plasma represents 55% of the blood volume and consists of 90% water and 10% dry matter.

In our simulations blood density is equal to 1.057 g/cm^3 and since we consider blood to be a Newtonian fluid, viscosity is constant with respect to shear rate and is equal to 3.5 cP.

3. Physiological Velocity Waveform

For the purpose of our simulations blood flow at the zone of interest is considered fully developed and is hence represented by a parabolic profile (Poiseuille flow) as follows:

$$u = U_{\max}(t)\left(1 - \frac{r^2}{R^2}\right) \tag{5}$$

Where u is the instantaneous velocity at a point of radius r.

U_{max} is the maximum instantaneous velocity in $\frac{cm}{s}$

R is the radius of the artery in cm.

In a 3-D model, the above equation results in a paraboloid at the inlet surface. But to replicate flow pulsatility we had to multiply the above equation by a time curve that represents the physiological waveform of blood flow in the left main coronary artery. For this purpose, we use a physiologically inspired triphasic waveform with an average Reynolds number equal to 240 and a Womersley[2] parameter equal to 2.8 as described in He and Ku (1996) [47]. A similar waveform was used by Feldman et al (2002) [67]. The normalized curve is shown in Figure 1 and the flow rate at

[2] Womersley parameter is the ratio of unsteady forces to viscous forces ($\alpha = \frac{d}{2}\sqrt{\frac{\omega}{\nu}}$, where d is the diameter, ω is the pulse rate, and ν is the viscosity)

maximum forward flow is equal to 300 $\frac{ml}{\min}$. The waveform includes backward flow for about 3% of the pulse period.

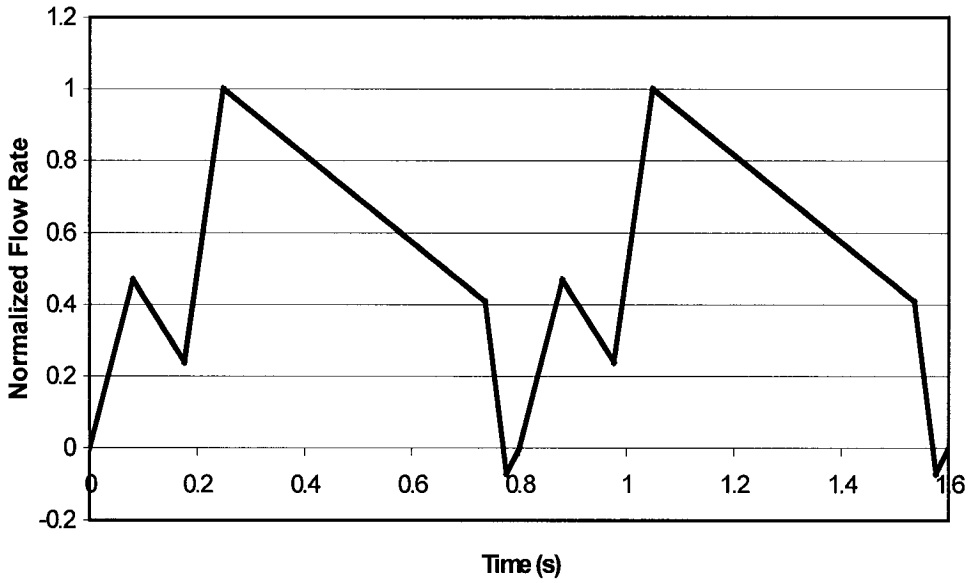

Figure 1: Normalized velocity waveform for the human left coronary artery flow

4. Shear Stress

In most hemodynamics studies, shear stress is the primary physical quantity of interest. It is also the main physical quantity used by different groups to establish correlations between the alterations to hemodynamics and the development of ISR. For a Newtonian fluid, shear stress is determined as the product of viscosity and shear rate. In our study, shear rate is calculated using the second invariant of the shear rate tensor, which accounts for pure shear as well as elongational deformation in the flow domain:

$$Shear\_Rate = (2S_{ij}S_{ij})^{1/2} \tag{6}$$

where S_{ij} is the strain rate tensor given by:

$$S_{ij} = \frac{1}{2}(u_{i,j} + u_{j,i}) \tag{7}$$

Chapter 5: Development of Numerical Models

1. CFD Modeling

CFD modeling allows the characterization of flow patterns that most experimental methods are not sensitive enough to discern, especially in the near-wall region. CFD involves the discretization of the fluid domain into small cells to form a grid. This allows the conversion of the governing partial differential equations into algebraic equations that can be solved numerically. The Finite Element Method (FEM) and the Finite Volume Method (FVM) are the two main discretization methods in CFD. O'Callaghan et al [68] compared the two methods for a femoral artery model and found that they are qualitatively similar. They also found FVM to give a slightly closer approximation to theory while FEM was significantly faster and required less computational memory.

In this study we use the Finite Element Method to carry out the CFD simulations. Gambit 2.1 (by Fluent Inc.) was used to generate the mesh for a geometric model exported from ProE (by PTC). Then FIDAP 8.7.2 (by Fluent Inc.) was used to apply boundary and initial conditions, to specify fluid properties, and to solve the governing equations. It was also used in conjunction with FIELDVIEW (by Intelligent Light) for postprocessing and viewing the results.

2. Stent Geometry

All the geometries used in this study were based on an experimental stent developed by SymbioTech Inc. (Quebec city, QC). The deployed configuration of the stent is shown in Figure 2 and a flat representation of the stent is shown in Figure 3. This stent has a slotted-tube design with consecutive closed cells in the form of positive hexagons followed by inverted hexagons with eight cell units around the circumference of the stent. This geometry can also be viewed as sequential sinusoidal rings with peak-to-peak connections, followed by only two peak-to-valley connections around the circumference, followed by valley-to-valley connections, followed by another inter-ring space with only two peak-to-valley connections around the circumference, and this pattern is repeated for the rest of the stent. The closed cells would provide the required strength for the stent and the space with only two periodic connections would provide the required flexibility.

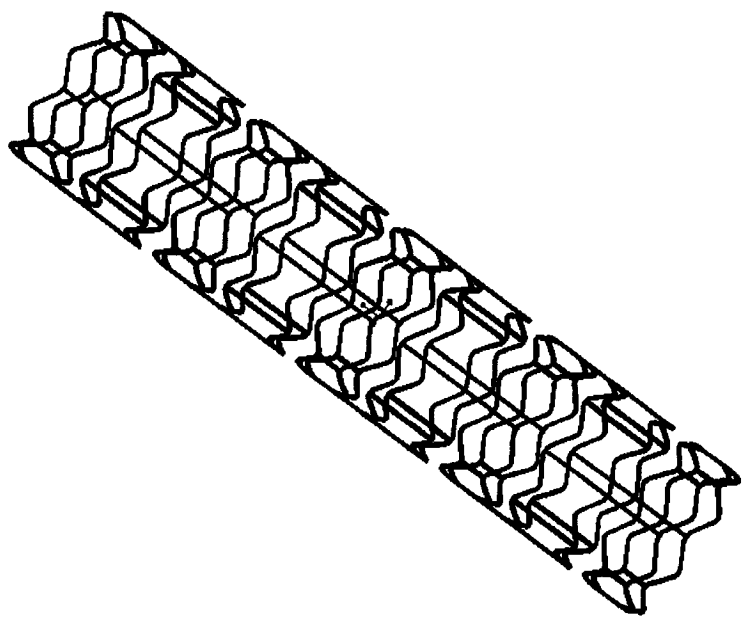

Figure 2: 3D Geometry of a coronary stent by SymbioTech Inc.

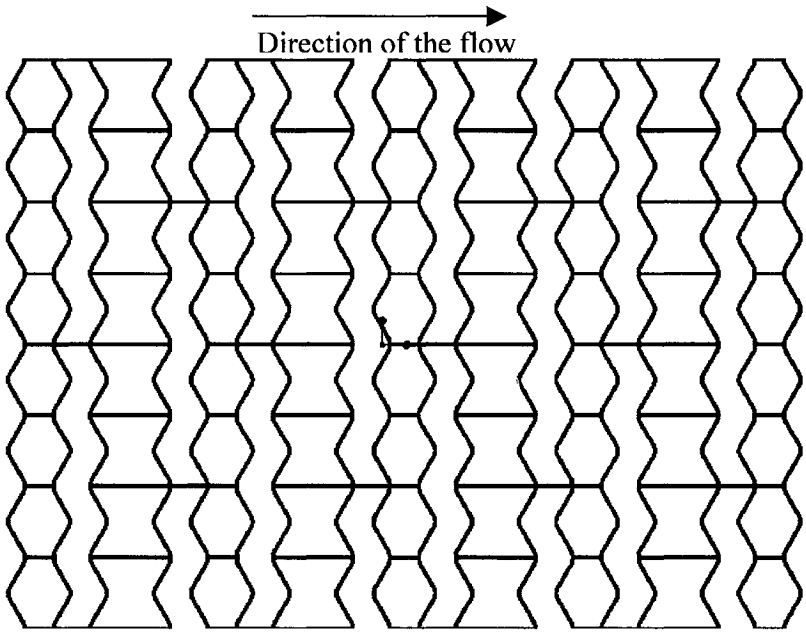

Figure 3: Geometry of the SymbioTech stent in a flat configuration

3. Two-Dimensional Models

The objective of creating 2D models is, first, to compare the results with those of the 3D models, and eventually analyze how this simplification affects the flow results. This is particularly important since a number of the previous studies have used 2D models for their simulations [61-63]. Therefore, this comparison can be helpful in evaluating the level of accuracy of their results and how they differ from those of a more realistic model, and eventually allow us to analyze our results in light of theirs. In addition, based on this comparison, 2D models can be used to carry out particular investigations that can be computationally very costly using 3D models but do not necessarily require the level of accuracy produced by 3D modeling.

3.1. Geometry

The 2D geometrical model is the representation of a planar section cut in the longitudinal direction of the stented coronary artery. The cutting plane is shown in Figure 4. Using symmetry, only half of the vessel was modeled. The artery has a diameter of 3mm, the struts have a dimension of 64 μm, and strut spacing was determined by the choice of the section cut and varied along the stent.

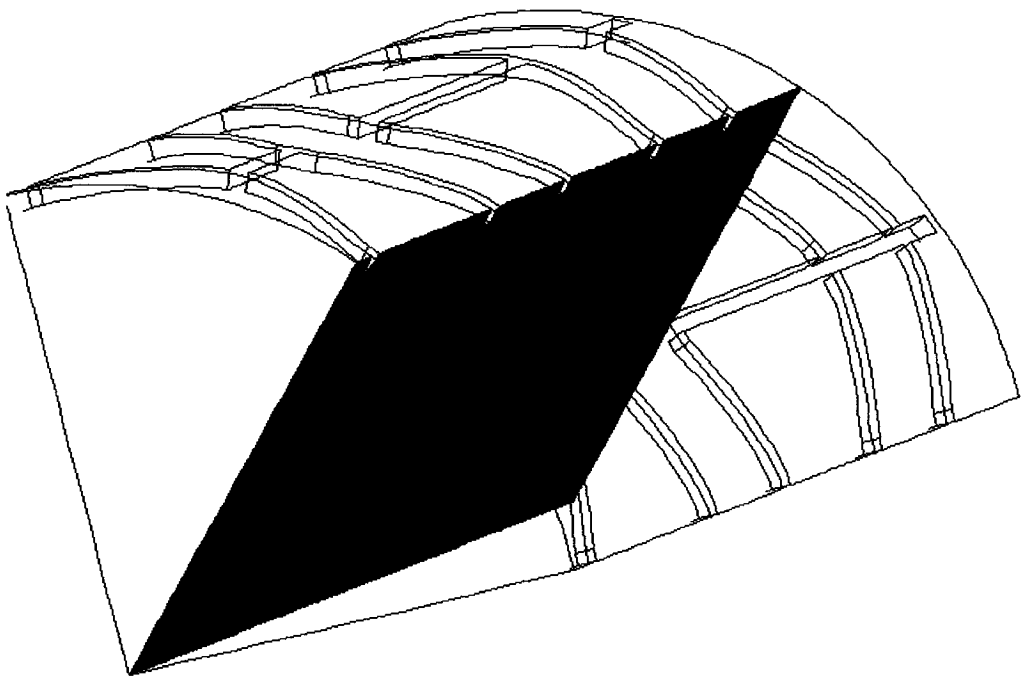

Figure 4: Cutting plane for 2D section definition

3.2. Mesh

The grids generated for this 2D model was constituted of quadrilateral linear elements. A mapping scheme was used to generate the mesh in the area closer to the stent struts since, in this case, this scheme gives better quality elements both in terms of skewness and aspect ratio A pave scheme is used for the rest of the lumen. However, to allow the use of the map scheme we had to subdivide the computational domain into several faces that are then meshed separately. The subdivision was made between the inter-strut areas, smaller areas in the region of the lumen close to the struts, and the rest of the lumen. Pre-meshing of the edges was also used to ensure satisfactory mesh density especially in the near wall region since it is the main zone of interest and the one expected to exhibit the highest gradients of the different flow parameters. The resulting mesh has 4858 nodes and 5038 elements and it is shown in figure 5.

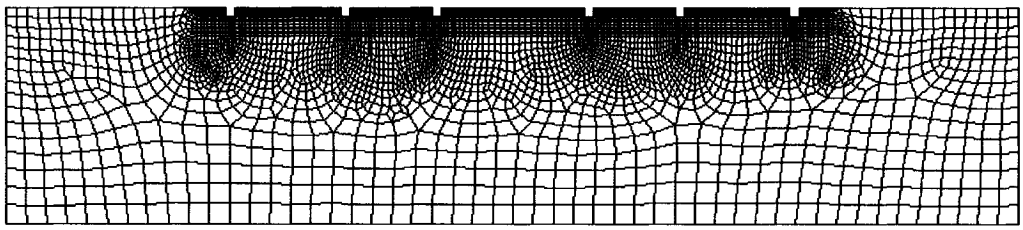

Figure 5-(a): **Mesh of the entire stented artery model**

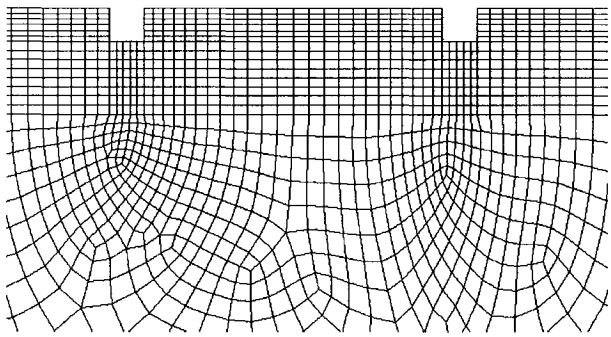

Figure 5-(b): Mesh of in the near wall region

Figure 5: 2D Mesh using a combination of map and pave schemes

3.3. Boundary Conditions

The boundary conditions applied to the 2D model involved:

- No slip condition at the artery wall and stent struts.
- Symmetry condition at the symmetry line
- Parabolic inlet boundary condition that is varying with time according to a physiological waveform of the coronary arteries.
- Zero pressure at the outlet

The boundary entities are shown in Figure 6 and the boundary conditions are summarized in Table 1.

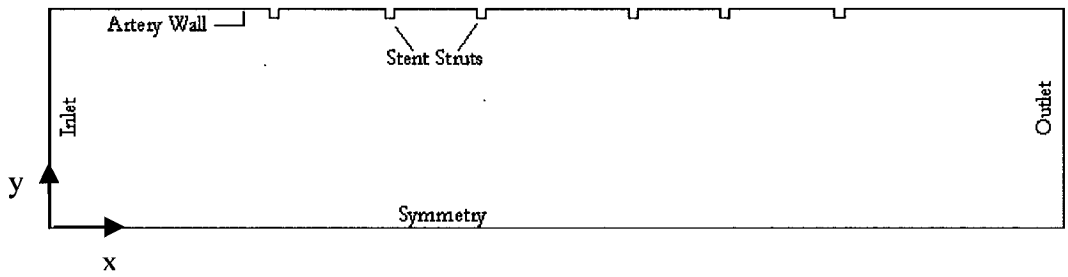

Figure 6: 2D Geometry and boundary entities

Boundary Entity	Boundary Condition
Artery wall Stent Struts	$u_x = u_y = 0$
Symmetry line	$u_y = 0$
Inlet	Parabolic and pulsatile velocity
Outlet	$P = 0$

Table 1: Boundary conditions for 2D models

3.4. Effect of Velocity Profile

Different cross sections along the coronary arteries exhibit different velocity profiles. Tang et al (1990) [69] for example have shown that, at the inlet of the left main coronary artery, blood coming from the sinus of Valsalva has a blunt velocity profile. He and Ku (1996) [47] show how this profile changes with for different positions

along the coronary artery. Therefore, to gain an understanding of how this limitation will affect our results, we ran three simulations using different inlet velocity profiles. The value of the velocity at the centerline, which is the section's maximum velocity, was changed to produce the same blood flow for the three profiles. These profiles were hence defined by the following equations:

- Parabolic profile: $u = U_{\max}\left(1 - \frac{r^2}{R^2}\right)$ (8)
- Blunt core profile: $u = \frac{2}{3}U_{\max}\left(1 - \frac{r^6}{R^6}\right)$ (9)
- Uniform velocity profile: $u = \frac{1}{2}U_{\max}$ (10)

These equations generate the profiles shown in figure 7:

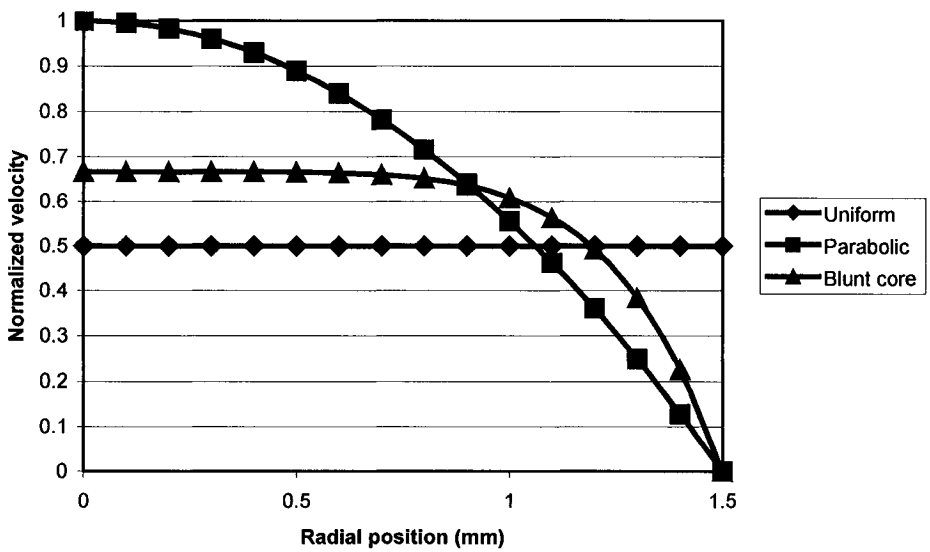

Figure 7: Inlet velocity profiles

4. Three-Dimensional Models

4.1. Geometry

The three-dimensional geometry represents the lumen of a coronary artery, 3 mm in diameter, with the struts of the SymbioTech Stent protruding into the lumen. In order to reduce the computational cost of our model, only one periodic unit of the stent geometry in the longitudinal direction is modeled. In addition, given that the geometry of the stent exhibits cyclic symmetry in the circumferential direction, only one quarter of the artery is modeled.

This geometry was generated using ProE by creating a cut on the lumen using the stent solid. A small volume in the center of the artery was then removed to allow the use of periodic boundary conditions in the side planes. The final geometry is shown in Figure 8

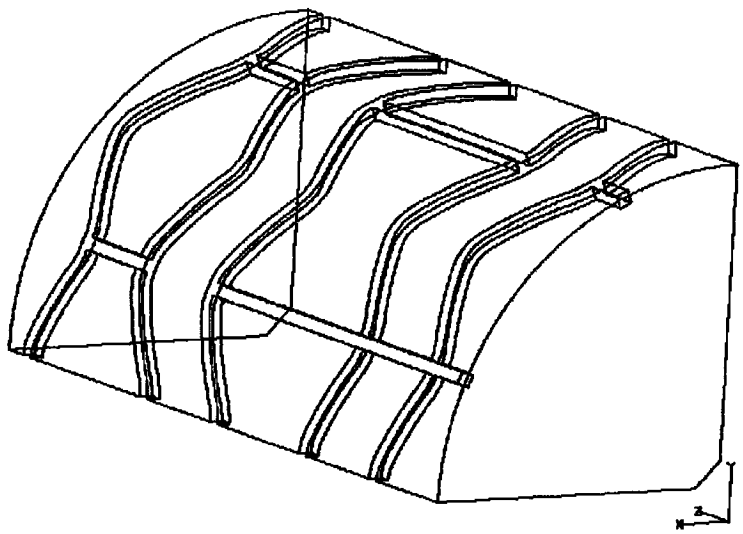

Figure 8: 3D Model of stented artery

4.2. Mesh

The 3D Mesh was generated by subdividing the volume of the lumen into several volumes, each volume representing an inter-strut space, plus one volume representing the rest of the lumen. This subdivision allowed the use of a map scheme with hexahedral linear elements for each volume separately. However, the side faces of the volume representing the bulk of the lumen were meshed using a Pave scheme. Boundary edges in these faces were pre-meshed with successively decreasing element size from the center of the lumen towards the arterial wall to ensure higher mesh density in the near-wall region. Manual pre-meshing of the edges was also necessary to ensure an adequate number of elements in the final mesh. Furthermore, the two side planes had to be topologically equivalent to allow the use of periodic boundary conditions. A typical resulting mesh is shown in Figure 9.

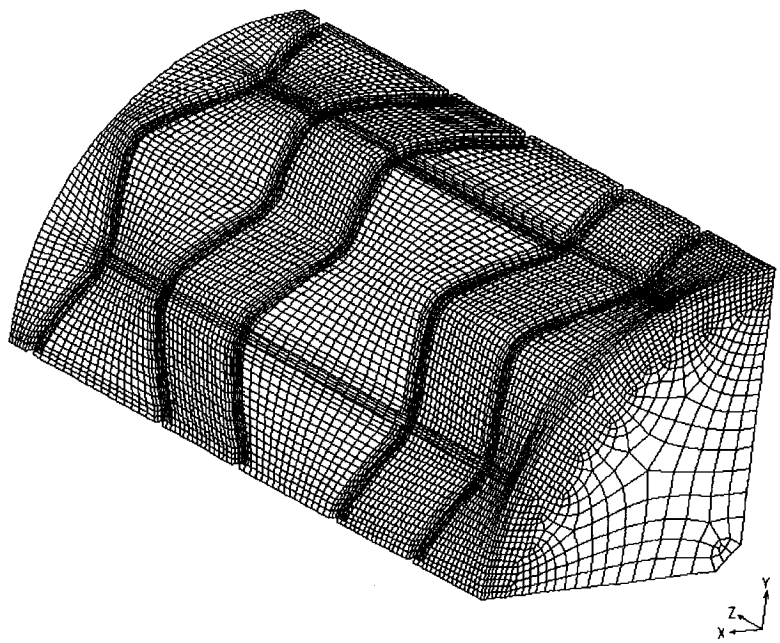

Figure 9: 3D Mesh with mapped hexahedral elements

4.3. Mesh and Temporal Resolution Independence

The most important challenge in obtaining accurate results in 3D problems is to ensure sufficient spatial resolution. In fact, mesh-independence is a necessary condition for the validity of the velocity and shear stress fields obtained from the computations. It is important to note though that a mesh resolution that produces accurate velocity results does not necessarily produce accurate WSS results. This is mainly due to the fact that WSS is a lower order computed parameter[70]. Therefore, to gain confidence in the shear stress results they have to directly be shown to be mesh-independent.

In our study, four meshes with different densities were used to evaluate the mesh-independency of our results. Moreover, to specifically ensure an increase in the accuracy of shear stress computations from one mesh to another, the number of elements in the strut sides and by consequence in the inter-strut region is increased systematically as shown in Figure 10.

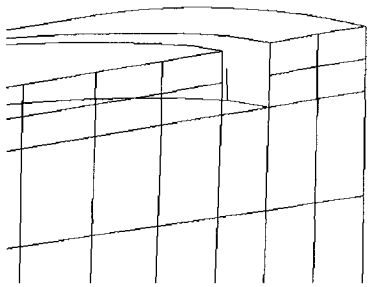

(a) Mesh 1

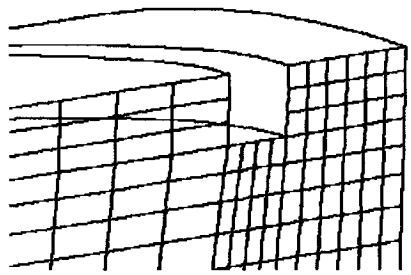

(b) Mesh 2

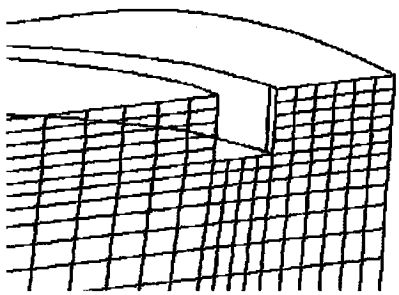

(c) Mesh 3

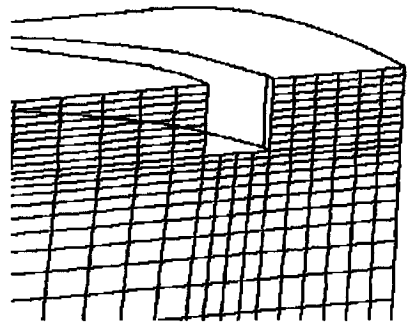

(d) Mesh 4

Figure 10: Mesh independence analysis

The following Table summarizes the characteristics of the different grids:

Mesh	Number of Elements	Number of nodes	Number of elements in the strut side
Mesh 1	29171	25878	2
Mesh 2	104182	95842	3
Mesh 3	191271	177369	5
Mesh 4	250657	233040	9

Table 2: Different grid intensities for mesh independence analysis

The number of discrete time integration steps used in the analysis is another simulation parameter that can affect the accuracy of the results. Therefore, to ensure the results independence of changes in the time step, different simulations with different time steps (8, 4, and 2 μs) were run and their results compared.

4.4. Boundary Conditions

The boundary conditions applied included the following:

- Inlet Surface: Velocity in the longitudinal direction (Uz) was set to a parabolic profile that varies with time according to a physiological waveform as described in section 4.3 above. To help in the convergence of the computations Ux and Uy were set to zero in this surface.
- Outlet Surface: Pressure was set to zero to allow measurement of pressure differences in reference to this surface.
- Arterial wall and stent struts: Using the non-slip condition velocity in these surfaces was set to zero.
- Side Planes: Periodic Boundary conditions were applied to these surfaces requiring that the solution at each node in one surface be the same as that of an equivalent node in the other surface. To apply the Periodic BC's on these surfaces they had to be identified in FIDAP as "SLIP" faces, as opposed to "PLOT" as all the other boundary faces. Because of this, local coordinate systems in the intersection edges between SLIP and PLOT faces become

inappropriate for the defined velocity BC's. Therefore, we had to explicitly define appropriate coordinate system for these edges.

All the boundary conditions are summarized in the following table:

Boundary Surface	**Boundary Condition**
Inlet	u_z: Parabolic profile with Physiological waveform $u_x = u_y = 0$
Outlet	Pressure = 0
Artery wall & Stent struts	u = 0
Side Planes	Periodic BC's

Table 3: Boundary conditions for 3D models

More details about the boundary conditions are provided in appendix A.

4.5. Numerical and Time Integration Schemes

FIDAP uses the Galerkin method to transform the Navier-Stokes equation into a set of non-linear algebraic equations. To solve this set of equations we use a segregated approach since it is more cost-effective than the fully coupled approach given the large size of our model. In fact, the segregated approach requires more iterations than the coupled approach, but because of the large number of nodes in our model, these iterations will be less expensive and hence the total numerical cost of the

problem will be smaller for the segregated approach. The main characteristic of the segregated approach is that instead of creating a global system matrix, it decomposes it into smaller sub-matrices, each related to one of the conservation equations. Normally, FIDAP will then solve these smaller sub-matrices using direct Gaussian elimination. However, in our case, we used instead a conjugate gradient-based iterative method to solve these linear equations systems. The conjugate residual (CR) method is used for the solution of the symmetric matrices and the conjugate gradient squared (CRG) method is used for the solution of the non-symmetric equation systems. For a detailed description of these methods refer to Appendix B.

When using the segregated solution methodology, convergence is based solely on the following criterion:

$$\left\| \frac{U_i - U_{i-1}}{U_i} \right\| \leq \varepsilon$$

Where $\|.\|$ is the root mean square norm summed over all the equations for the model, U is the solution vector, and ε is the convergence tolerance. The criterion is applied separately to each degree of freedom being solved for and the solver considers convergence reached whenever the norms in the left hand side of the inequality above are all simultaneously less than less than the specified tolerance. Convergence tolerance in our model is set to 0.001 (refer to Appendix A) which is the recommended value for the segregated approach.

In addition since we are dealing with a transient problem, a time integration scheme is used in addition to the spatial discretization scheme to allow the integration of the solution field in time. In our model we use the first order backward Euler time integration scheme with a fixed time step.

5. Comparison With Healthy and Stenosed Arteries

3D models of healthy and stenosed arteries were created to investigate the differences in the hemodynamic parameters that the presence of a stent introduces into the artery (Figure 11 (a) and (b)). Simulations for these models were run using the same waveform for the inlet velocity.

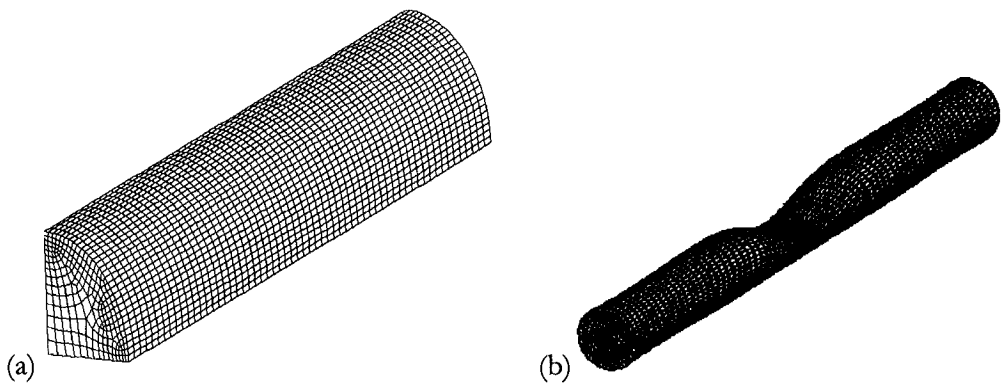

Figure 11: Healthy and stenosed artery models

Similar to the stented model, only one quarter of the healthy artery is represented. The stenosed artery model has a 50% eccentric stenosis. Therefore the whole artery had to be modeled. The stenosis has a biguassian profile, which is considered to mimic best the common shape of coronary stenosis.

Chapter 6: Numerical Results

1. Mesh Independence

The results from the different mesh resolutions were compared by plotting speed values and shear rate results along segments from the two lines defined in Figure 12 which lie on the section defined in Figure 4.

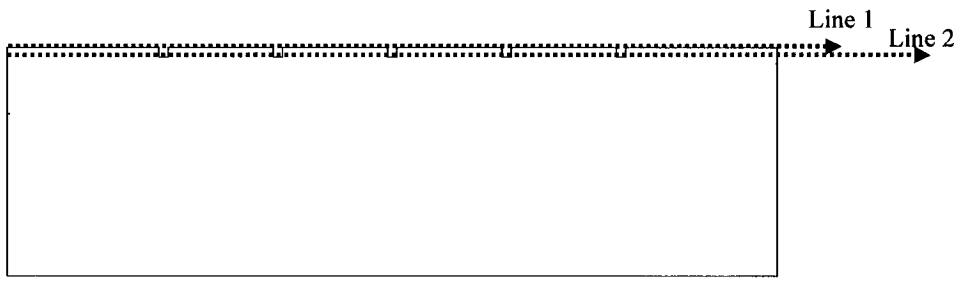

Figure 12: Plotting lines definition

For Line1, blood velocity is zero all along as a consequence of the no-slip condition. Therefore, velocity norm was plotted along a segment of Line2 between two struts and shear rate was plotted along a segment of Line1 between two struts and a segment of Line2 around one strut, for each of the four grids (Figure 13 (a), (b) and (c)).

The velocity norm curves show that a grid resolution as high as that of Mesh2 is sufficient for obtaining accurate velocity results. The error between Mesh 2 and mesh 4 all along the line is estimated to be less than 2%.

Along Line1 shear rate plots represent WSS distribution and along Line2 they capture the shear rate variations at the tip of the struts. These results show that, for WSS, a grid as fine as Mesh2 is enough to obtain mesh independence. However, for

the shear results at the tip of the struts, where shear gradients are the highest in the whole computation domain, a mesh resolution at least as high as Mesh3 is needed.

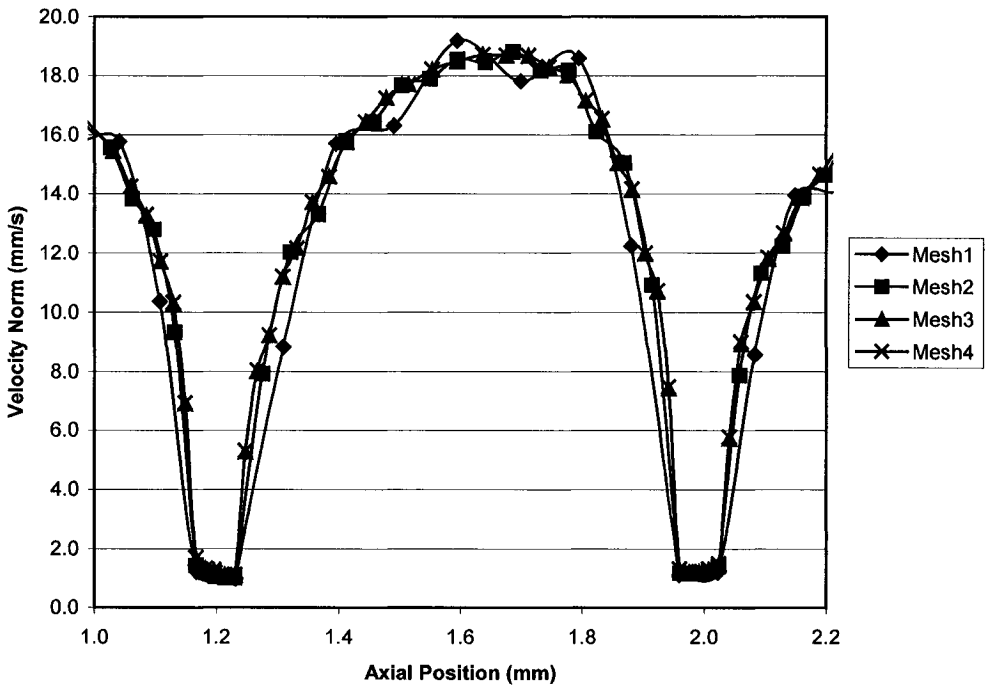

Figure 13-(a): Velocity norm distribution along Line2 for different meshes

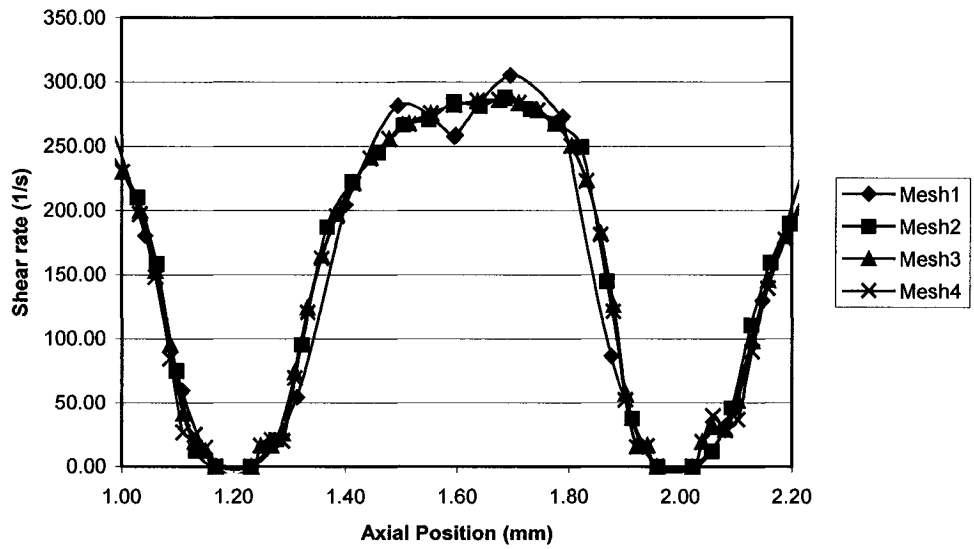

Figure 13-(b) Shear rate distribution along Line1 for different meshes

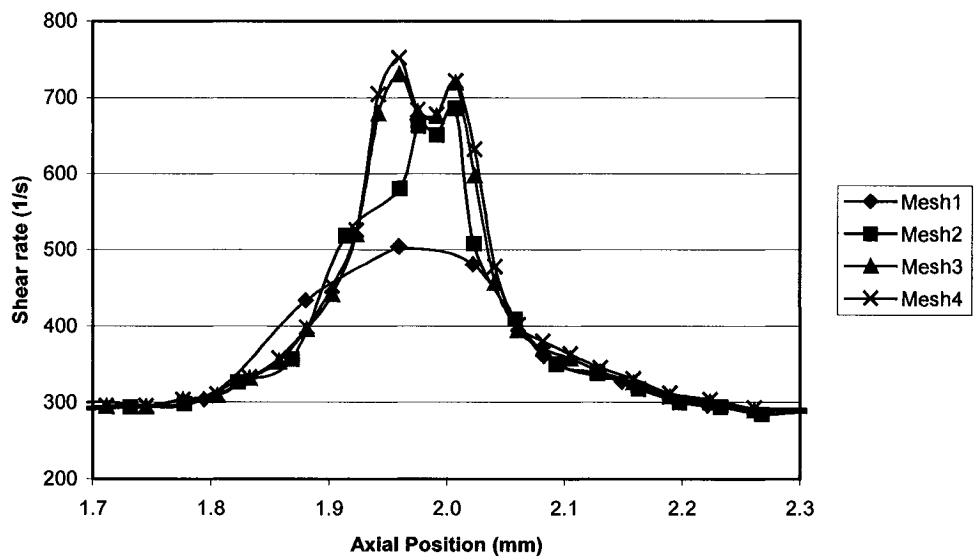

Figure 13-(c): Shear rate distribution along a segment of Line2 for different meshes

Figure 13: Mesh Independence results

2. Time Step Independence

Time variations for the velocity norm at a point midway between two struts and 64 μm away from the artery wall, and for wall shear rate at a point midway between two struts, was plotted for different time steps (Figure 13 a1,a2, b1, and b2). The results show that, for most of the pulse period, the time steps used are small enough to reach time step independence. However, to obtain accurate results of the velocity norm and shear rate fluctuations around the peack backward flow time, we need to use a time integration step smaller than 4 ms.

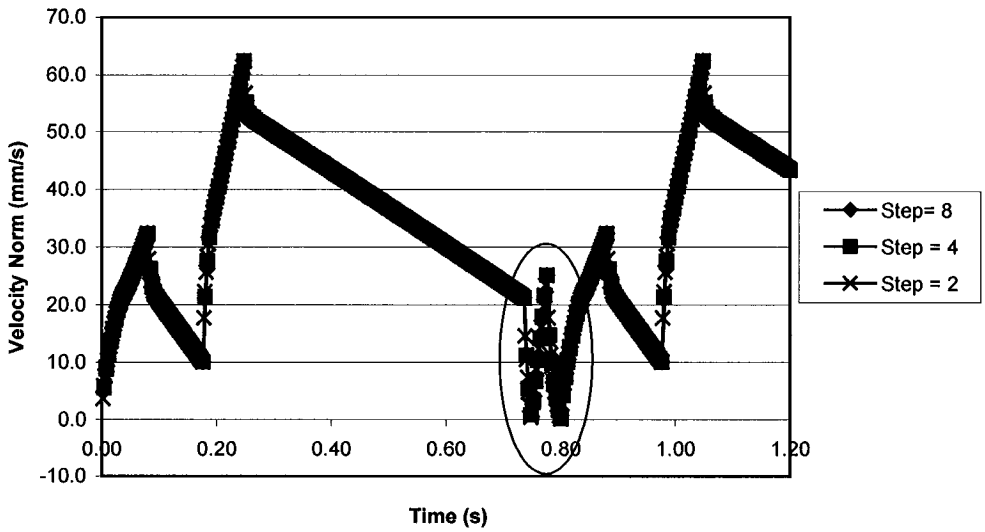

Figure 14-(a1): Velocity vs time for different time integration steps

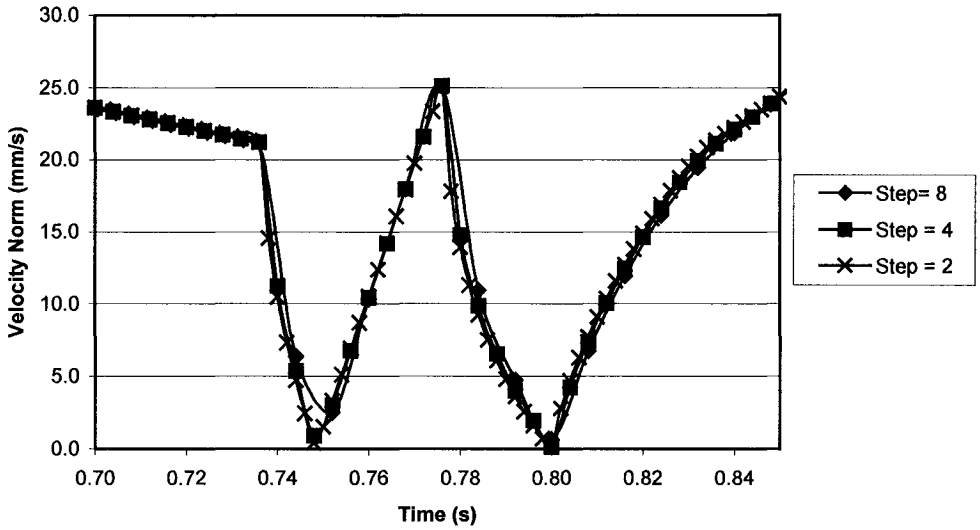

Figure 14-(a2): Zoomed in plot of circled zone in a1

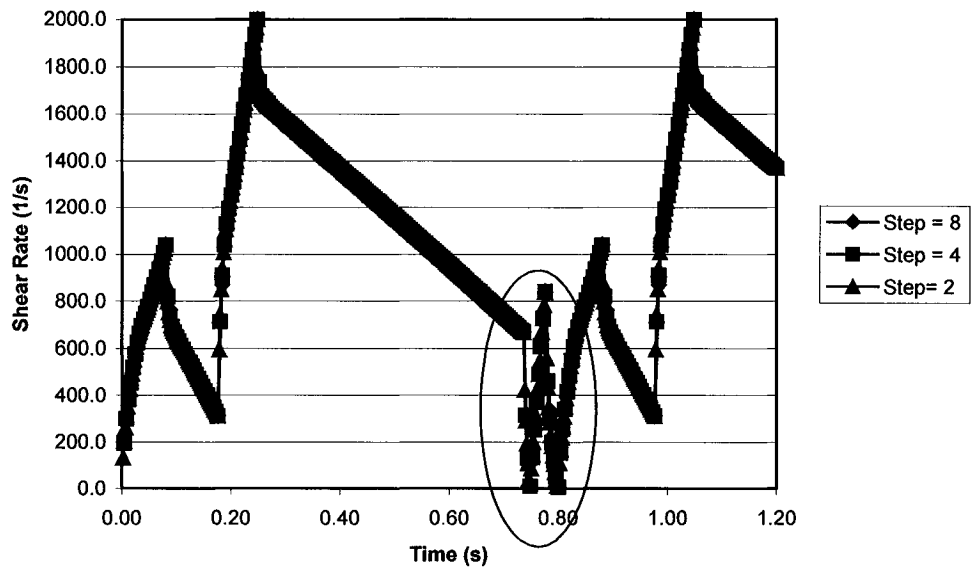

Figure14-(b1): Shear rate vs time for different time integration steps

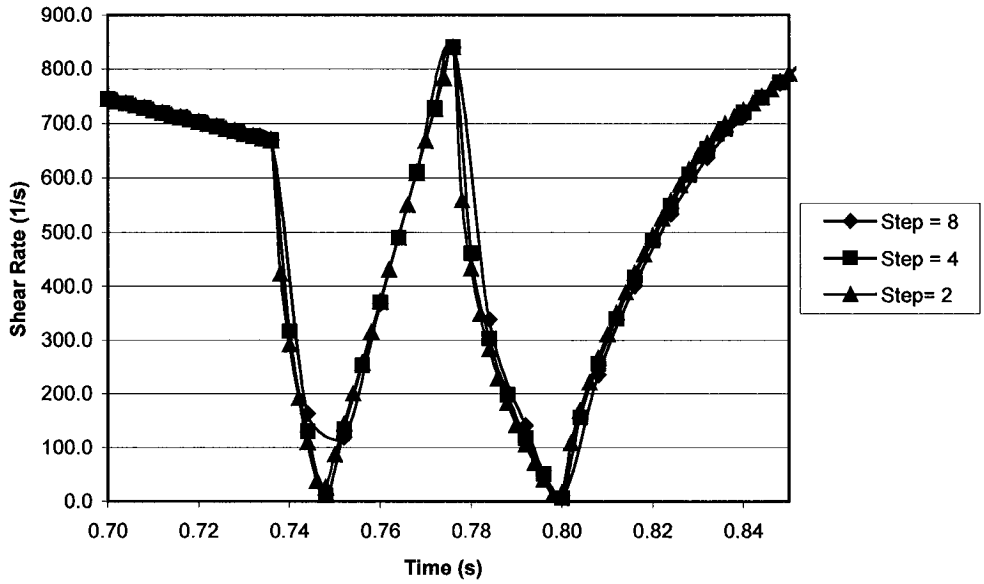

Figure 14-(b2): Zoomed in plot of circled zone in b1

Figure 14: Time step independence analysis

3. Effect of Inlet Velocity Profile on Hemodynamic Parameters

To compare the effect of the different inlet velocity profiles on the flow patterns and on the shear stress results in a stented artery we plot the velocity norm along Line1 and shear rate values along Line2 for the three profiles, as shown in Figure 15 (a) and (b).

These results show that the inlet velocity profile significantly affects the flow patterns and wall shear stress results within the stented segment of the artery. We notice however that the difference between velocity norms and shear rate values for the different velocity profiles decreases with each subsequent inter-strut zone in the direction of the flow. We also notice that the difference in wall shear rate is more

pronounced where the distance between the struts is higher. Finally, we notice that the more blunt the profile the higher the velocity and shear values for every inter strut zone.

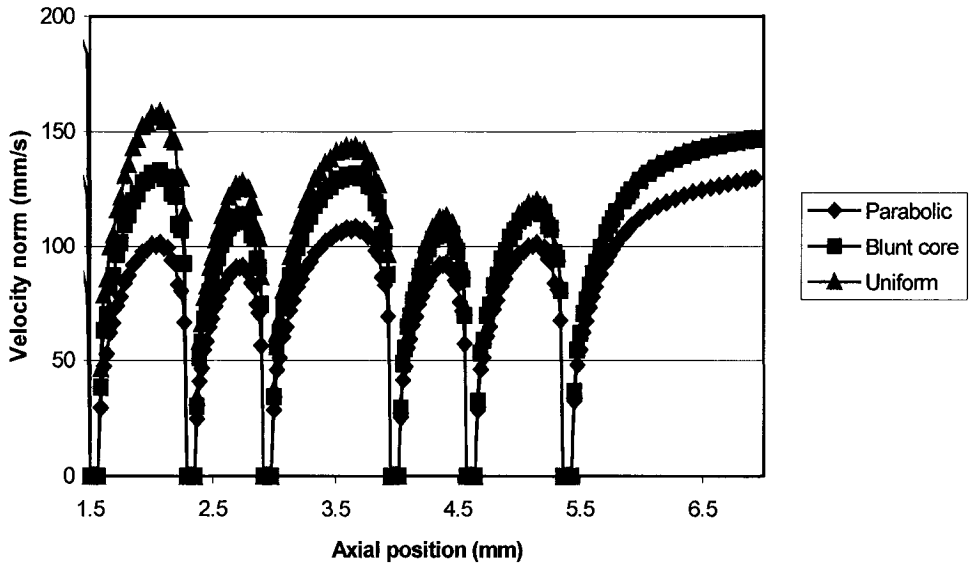

Figure 15-(a) Velocity norm along Line2 for different inlet velocity profiles

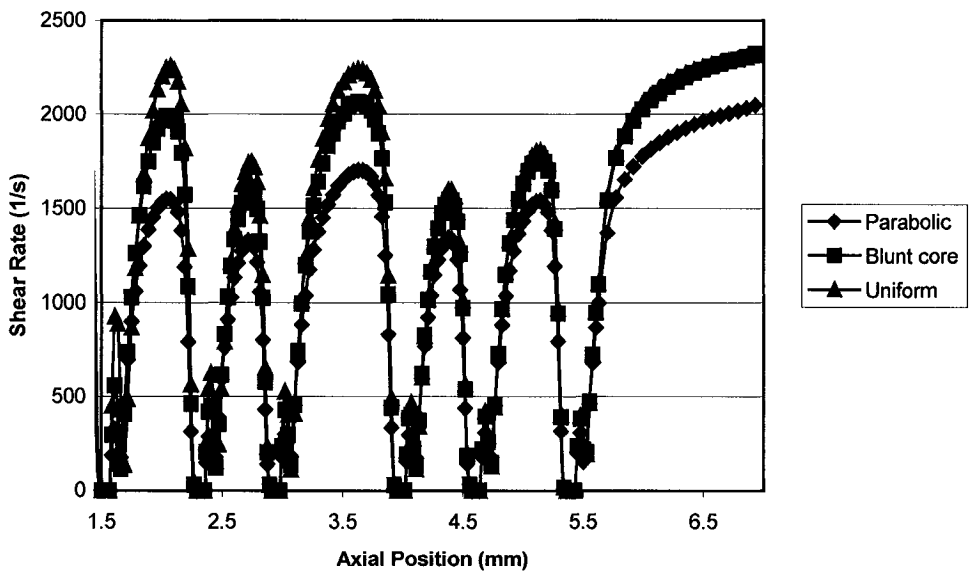

Figure 15-(b): Shear rate along Line1 for different inlet velocity profiles

Figure 15: Velocity norm and shear rate plots for different inlet velocity profiles

4. Comparison Between 2D and 3D Models

Velocity norm and shear rate results along segments of Line1 and Line2 for both the 2D and 3D models were plotted and superimposed for peak forward flow and peak backward flow conditions as shown in Figure 16 (a), (b), (c) and (d).

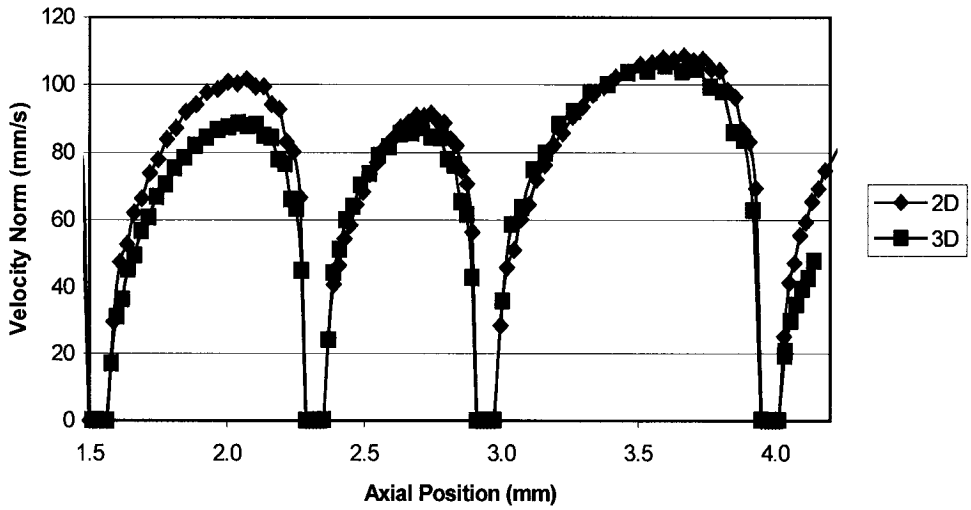

Figure 16-(a): Velocity norm along line 2 for 2D and 3D models at peak forward flow

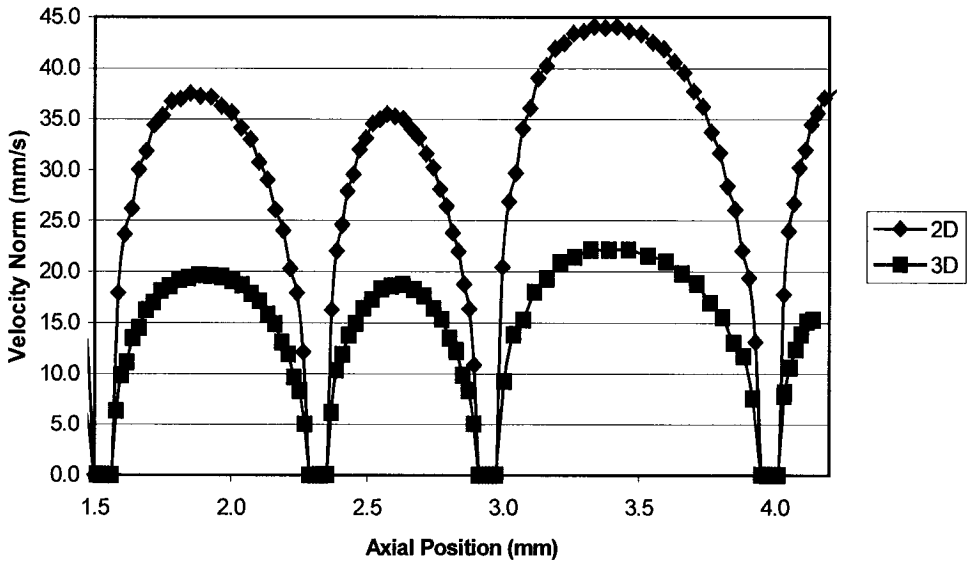

Figure 16-(b): Velocity norm along line 2 for 2D and 3D models at peak backward flow

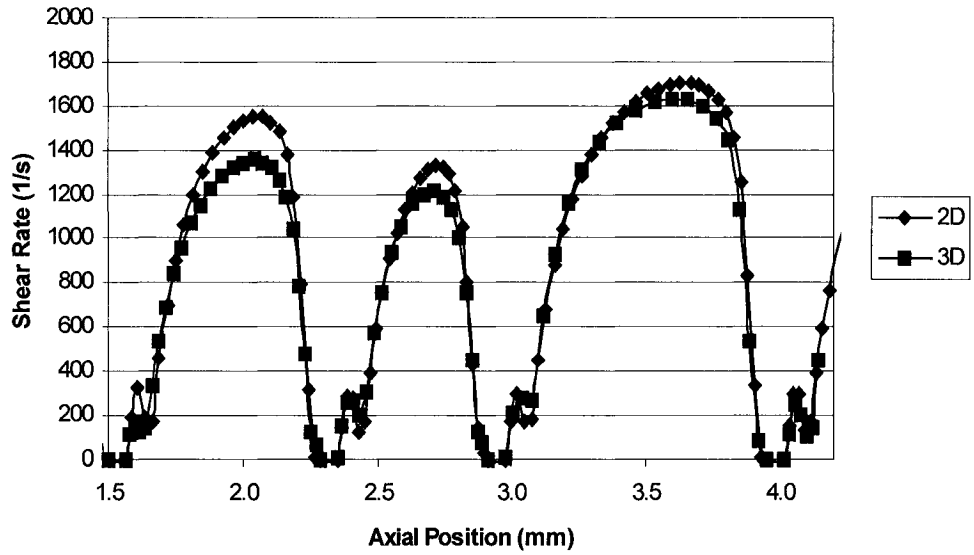

Figure 16-(c): Wall shear rate for 2D and 3D models at peak forward flow

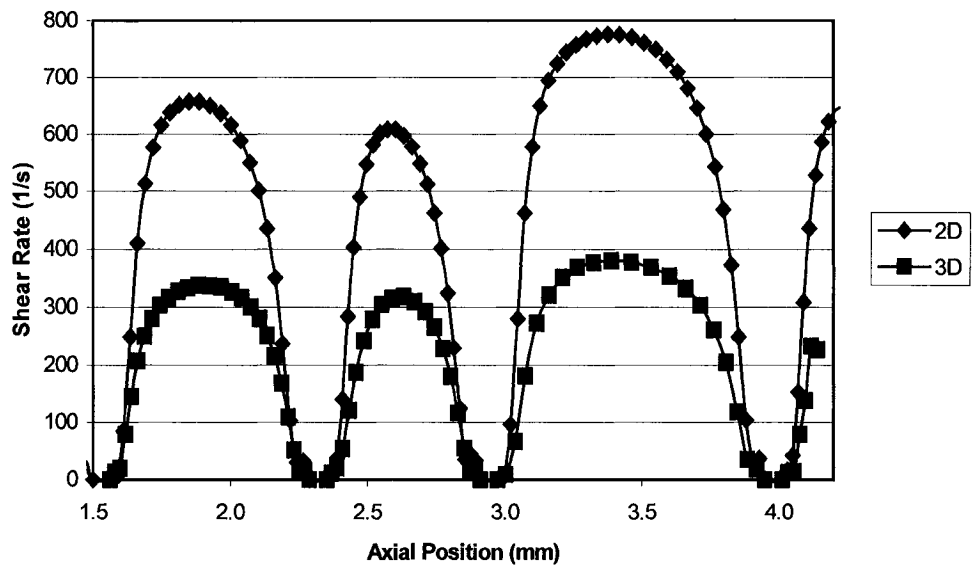

Figure 16-(d): Wall Shear rate for 2D and 3D models at peak backward flow

Figure 16: Comparison between 2d and 3D models

These results show that 2D models for most of the segments studied overestimate the values of both the velocity norm and the shear rate. However, we notice that for peak forward flow the difference between 2D and 3D results for both velocity and

shear do not exceed 16% and decrease systematically for each subsequent inter-strut zone in the flow direction, while for peak backward flow the difference is over 85% with no noticeable difference between the different inter-strut zones.

5. Secondary Flow

5.1. Projected Velocity Vector Fields

Secondary flow is the flow perpendicular to the principal laminar stream along the artery. In this case, it is the combination of the circumferential and radial flow components. Using the "Projected Vector" option in FIELDVIEW we were able to obtain the vector field of the secondary flow in different cross sections along the stent segment. Furthermore, the color-coding for the vectors was based on the magnitude of the projected vector given by $\sqrt{Ux^2 + Uy^2}$. The cutting planes used for defining the different cross sections are shown in Figure 17 and are 0.254 mm apart from each other.

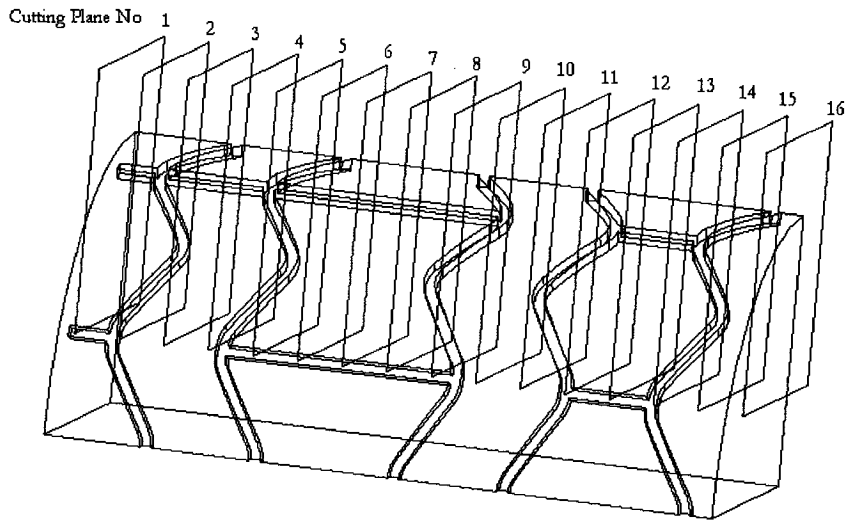

Figure 17-(a): Side view

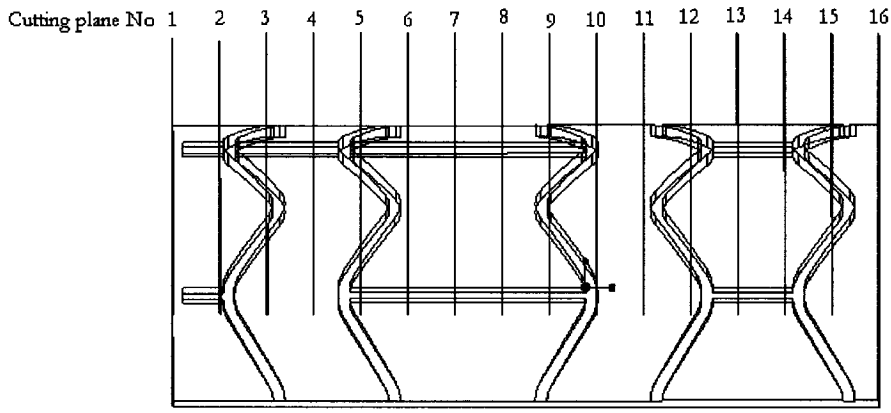

Figure 17-(b): Front view

Figure 17: Cutting planes for display of secondary flow

The vector fields of the secondary flow components are shown in Figure 18 (a) to (j) for cutting planes 4 to 13, at peak forward flow.

They show pronounced circumferential flow in the open cell structures, with the flow converging towards the center downstream of a peak and upstream of a valley of the sinusoidal rings (plane 4), and diverging away from the center downstream of a valley and upstream of a peak (planes 10 and 11). They also show the creation of vortices in the closed cell structures with opposite directions for the inverted hexagon and positive hexagon cells, following similar pattern relative to the peak and valley of the rings as described above (planes 6,7 and 13). We can also notice that secondary flow decreases significantly and is almost inexistent when we move away from the struts that are perpendicular to the main blood stream (plane 8). The radial component of the flow is shown, as expected, to be more pronounced towards the center of the artery upstream of the struts (plane 9) and towards the artery wall downstream of the struts (plane 10).

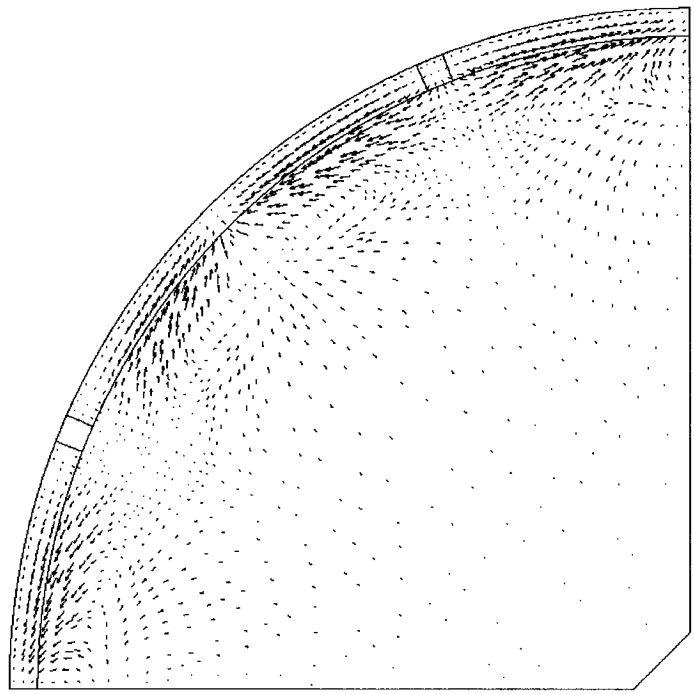

Figure 18-(a): Secondary flow on cutting plane 4

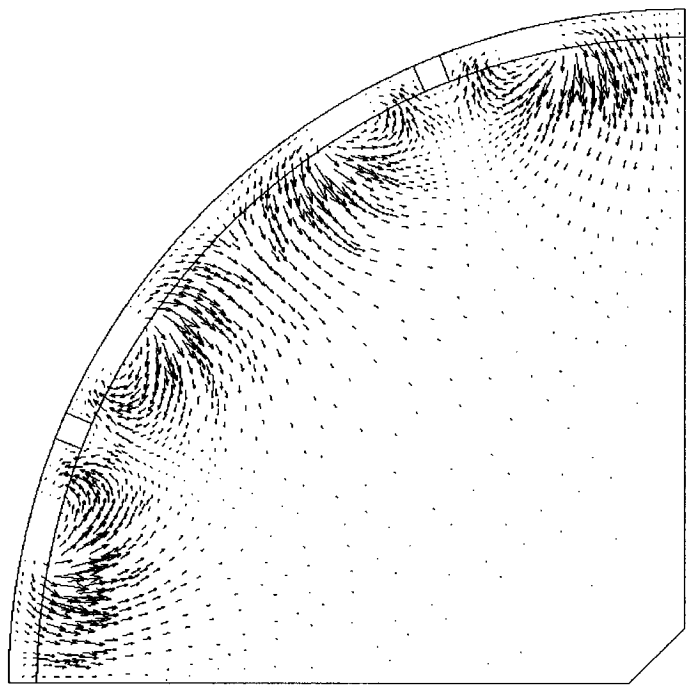

Figure 18-(b): Secondary flow on cutting plane 5

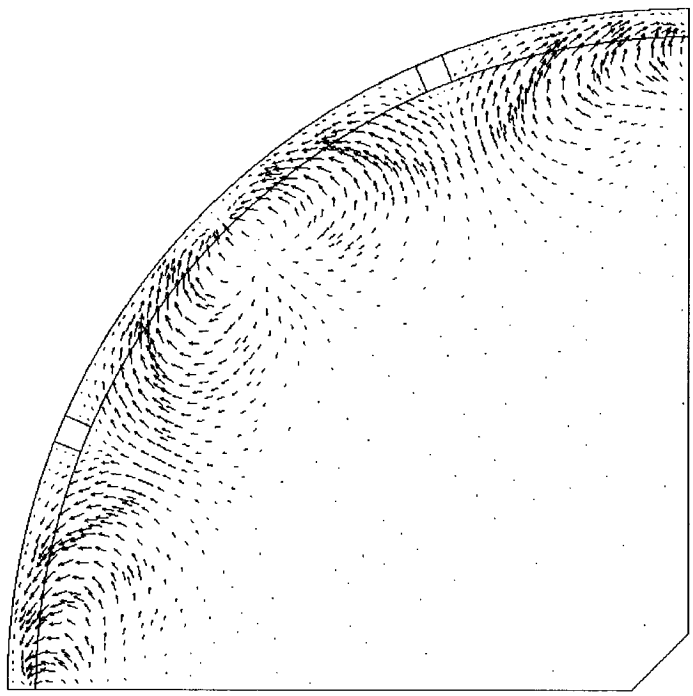

Figure 18-(c): Secondary flow on cutting plane 6

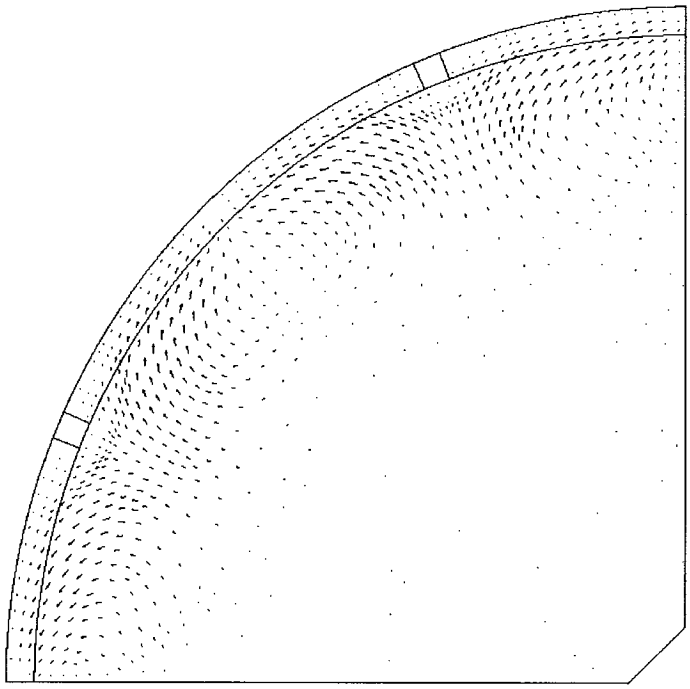

Figure 18-(d): Secondary flow on cutting plane 7

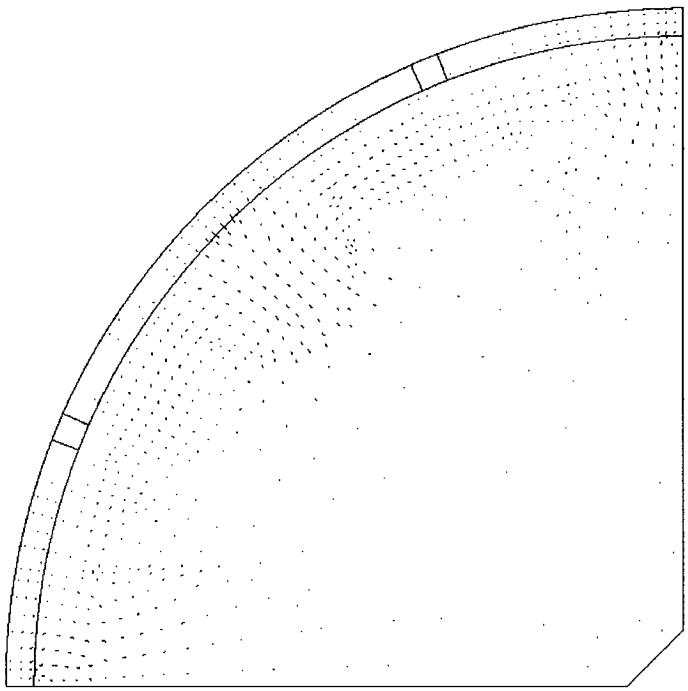

Figure 18-(e): Secondary flow on cutting plane 8

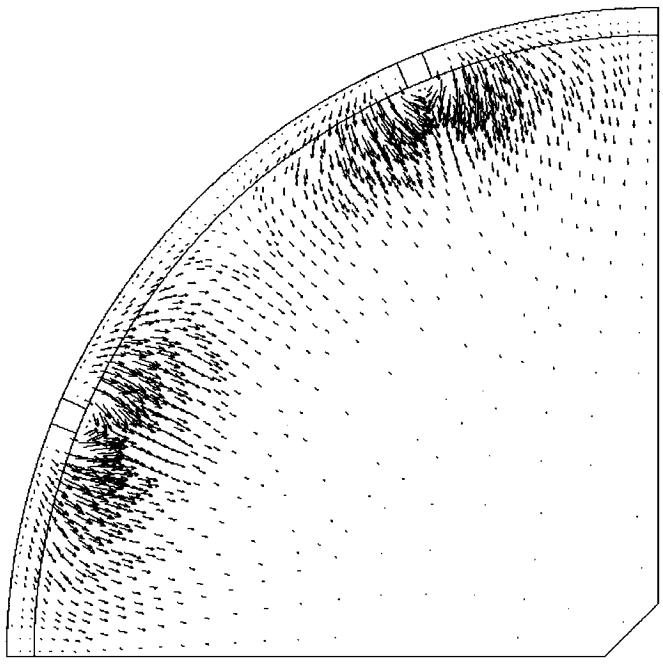

Figure 18-(f): Secondary flow on cutting plane 9

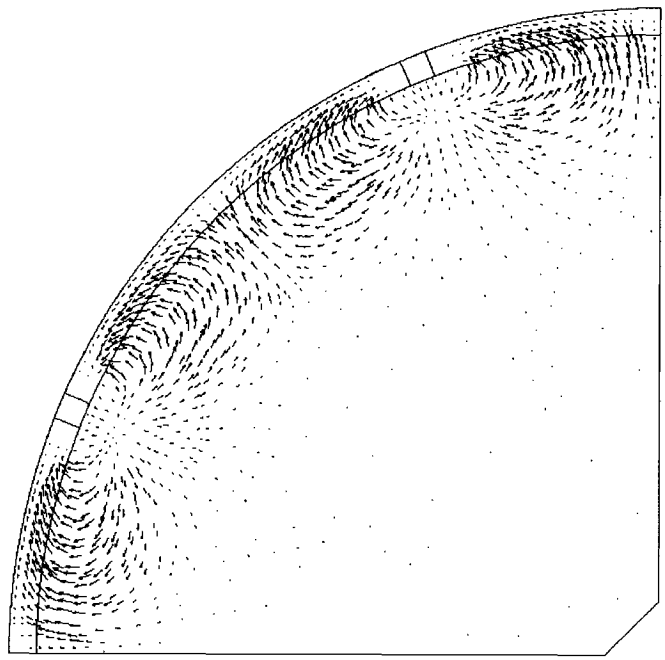

Figure 18-(g): Secondary flow on cutting plane 10

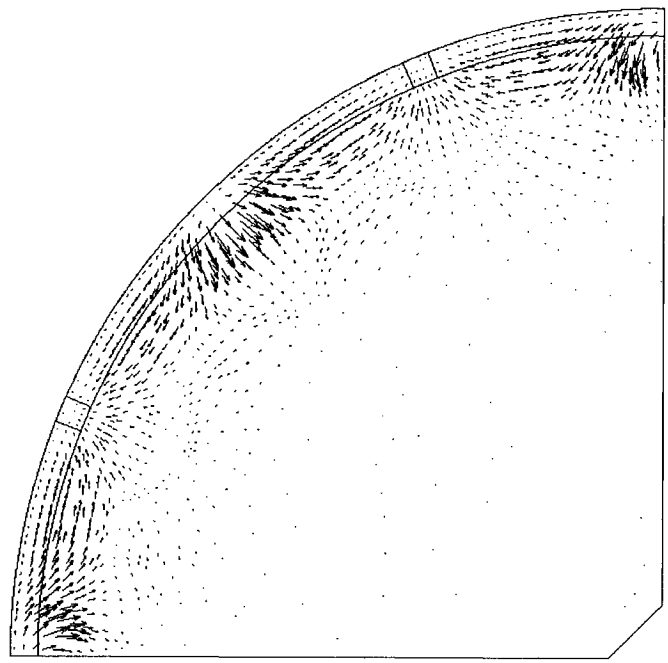

Figure 18-(h): Secondary flow on cutting plane 11

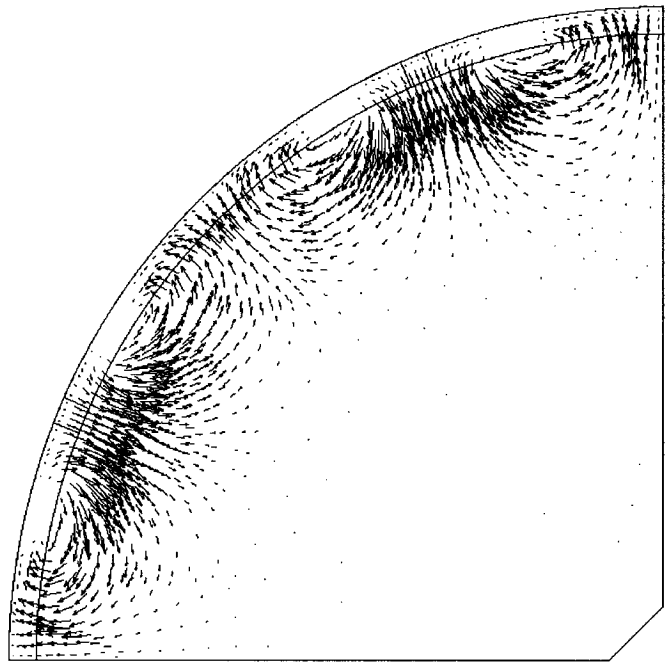

Figure 18-(i): Secondary flow on cutting plane 12

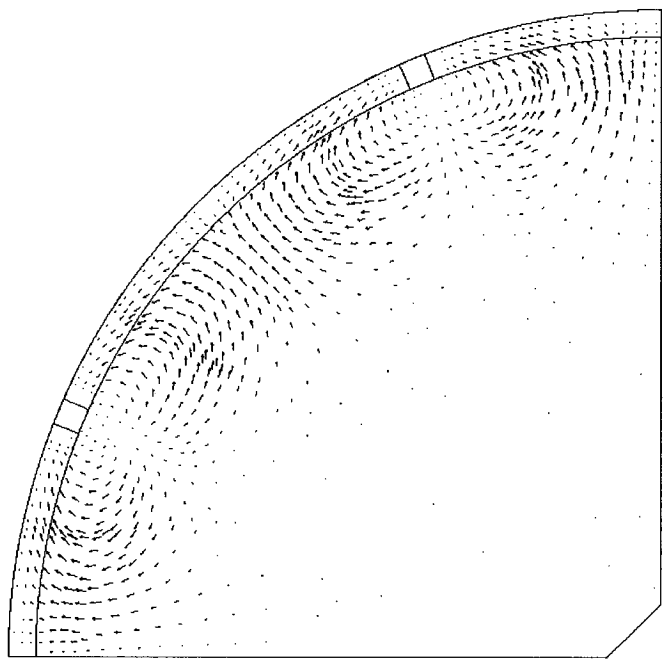

Figure 18-(j): Secondary flow on cutting plane 13

Figure 18: Secondary flows at different cross sections at peak forward flow

5.2. Velocity Streamlines

To gain a visual understanding of the link between the different planes plotted above and how they affect the flow as a whole, different streamlines emanating from equally spaced seed points located at the inlet surface at 12.5 μm from the artery wall were plotted and are shown in Figure 19.

The color-coding for these lines is based on the local value of the axial component of blood velocity. These streamlines show that the flow in the struts region converges towards the center of the inverted hexagon cells and diverges towards the sides of the positive hexagon cells. We also notice that the convergence is more pronounced with the presence of struts in the axial direction even if the velocity norm is reduced around these struts.

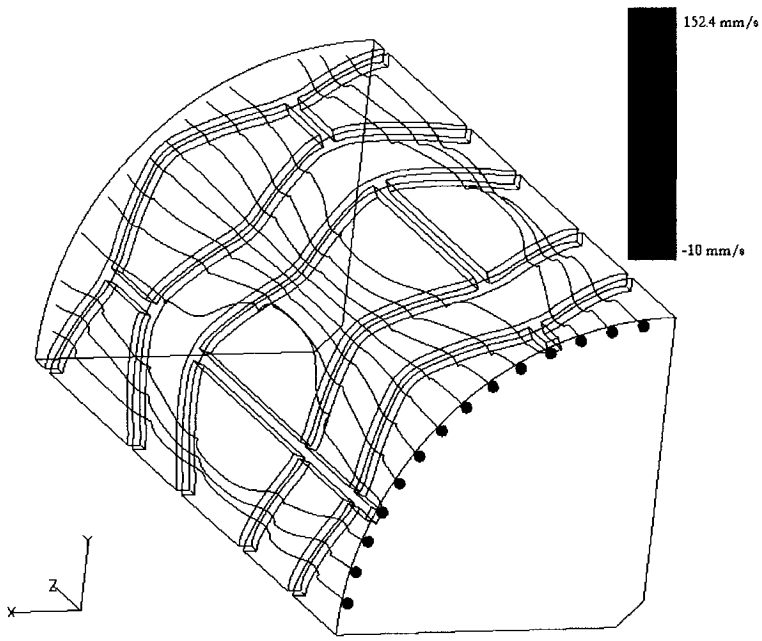

Figure 19: Velocity streamlines at the near wall region

5.3. Velocity Components

We also plotted the magnitude of both the secondary ($\sqrt{Ux^2 + Uy^2}$) and the axial ($|Uz|$) component of the flow velocity along Line2 at peak forward flow and peak backward flow. The resulting graph is shown in Figure 20. We can notice from this graph that secondary flow becomes a major component of the flow velocity as we get closer, both upstream and downstream, to the struts. Furthermore, the maximum value of secondary flow along the line reaches 32% of the maximum value of the axial component at peak forward flow and 30% at peak backward flow.

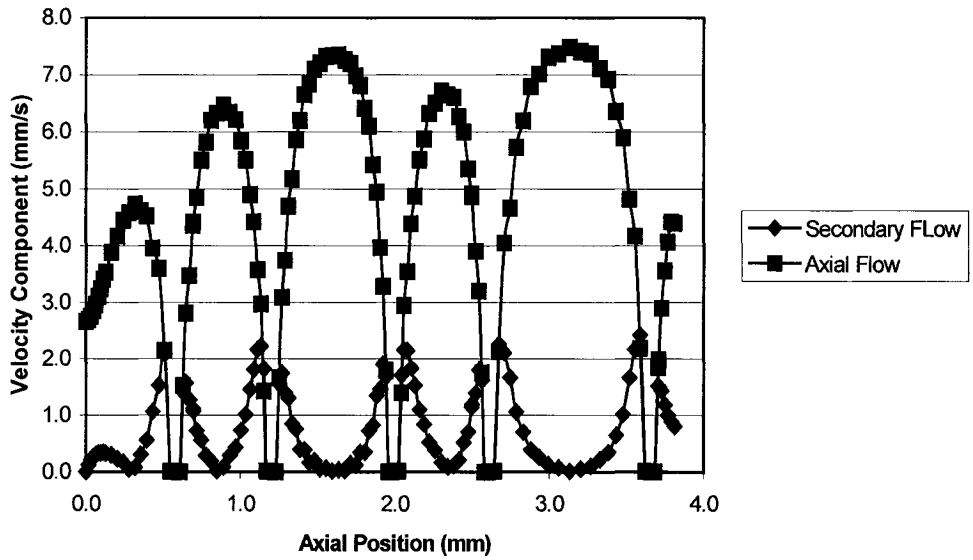

Figure 20-(a): Peak forward flow

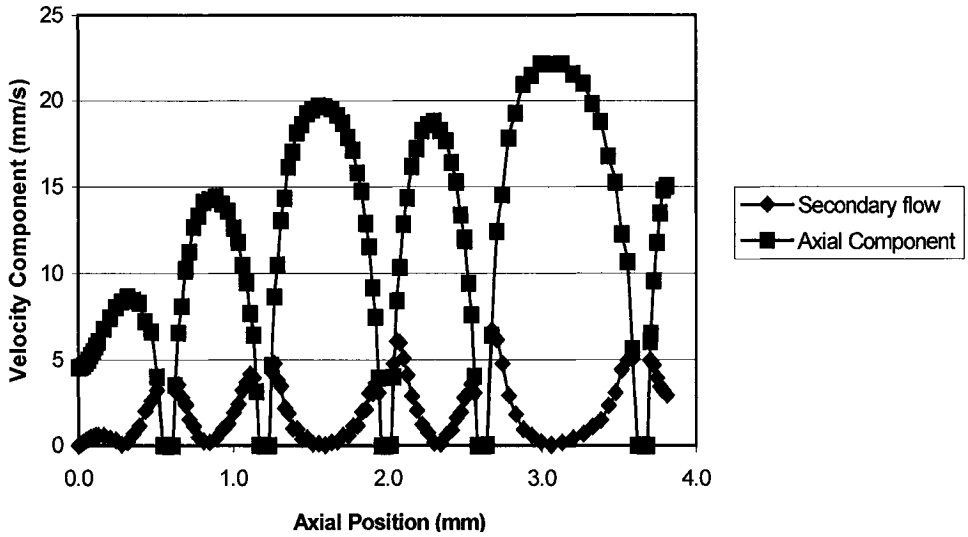

Figure 20-(b): Peak Backward flow

Figure 20: Secondary and axial velocity components at peak forward and backward flows

6. Shear Rate Distribution

To study the spatial distribution of shear stress in the stented segment of the artery, we plotted shear stress contours on the artery wall, the stent struts and in the blood as shown in Figures 21, 22, and 23.

The wall shear rate distribution shows areas of low shear rate around the struts. These areas are shown to be larger at the conjunction points and around the peaks and valleys of the stent's rings. This distribution also shows that at peak forward flow closed cell structures exhibit markedly higher values of wall shear rate compared to the open cells. It also shows that the presence of a connecting strut in the axial direction in the open cell structure results in an increase in the value of the wall shear rate. At peak backward flow, shear rate increases systematically from one inter-strut

spacing to the next in the main direction of the flow. The values of maximum shear rate are an order of magnitude less than those resulting at peak forward flow.

We can also notice that for peak forward flow, shear rate is much higher for the struts that are perpendicular to the flow compared to the ones that are in the direction of the flow. This can be due to the changes in flow direction across the struts that are perpendicular to the flow.

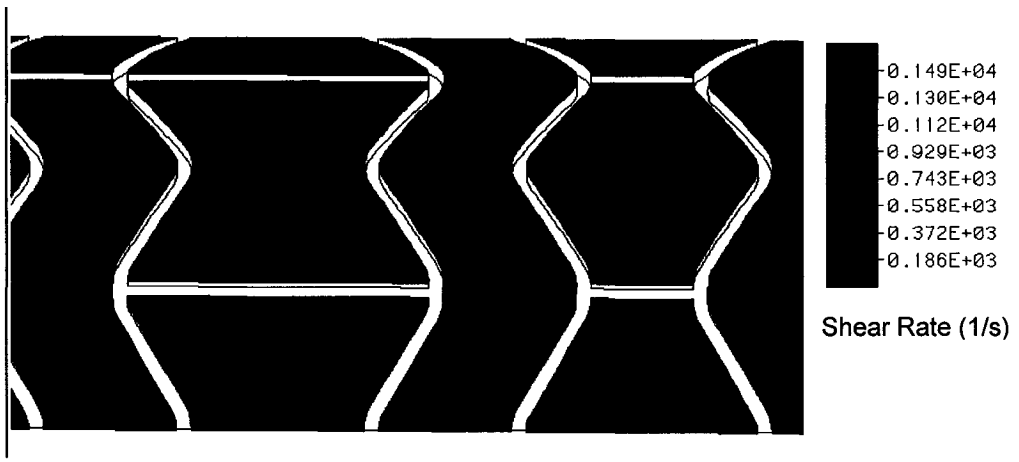

Figure 21-(a): Shear rate distribution in the artery wall at peak forward flow

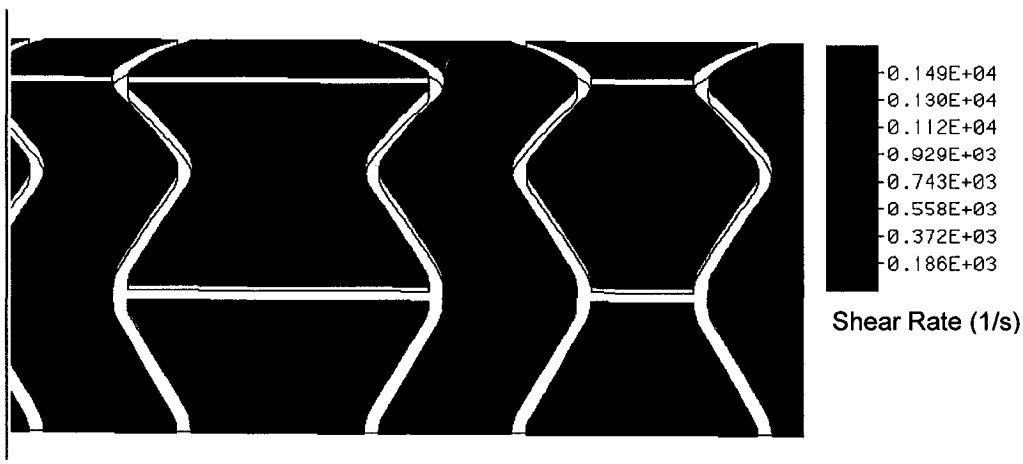

Figure 21-(b): Shear rate distribution in the artery wall at peak backward flow

Figure 21: Wall shear rate distribution for peak and forward and backward flows

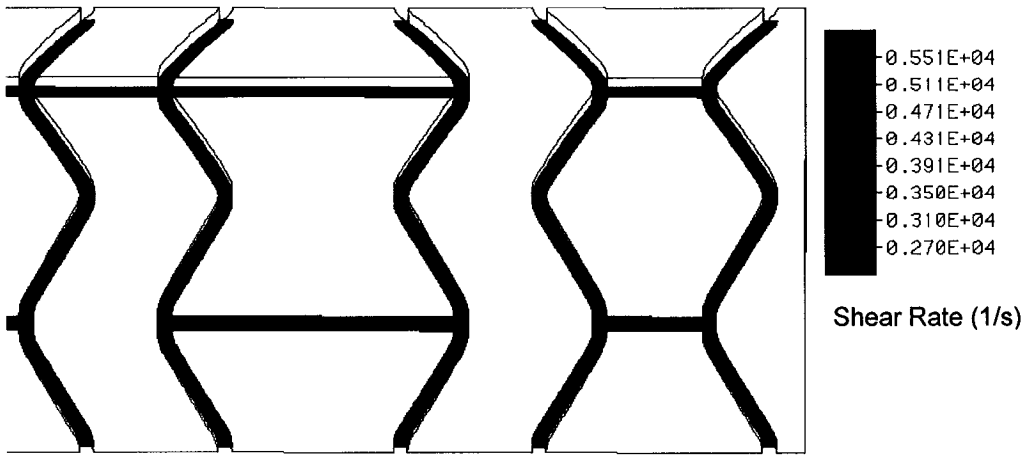

Figure 22-(a): Shear rate distribution in the struts tip at peak forward flow

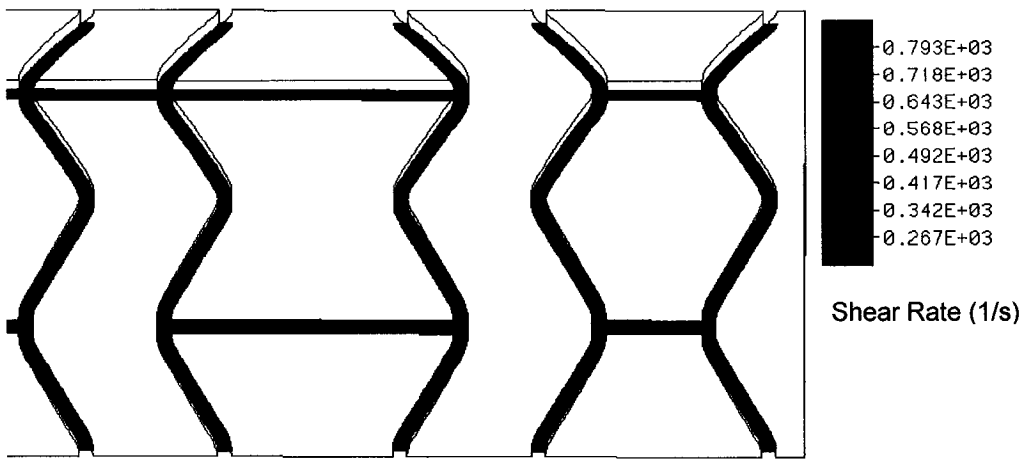

Figure 22-(b) Shear rate distribution in the struts tip at peak backward flow

Figure 22: Shear rate distribution at the tip of the struts at peak forward and peak backward flows

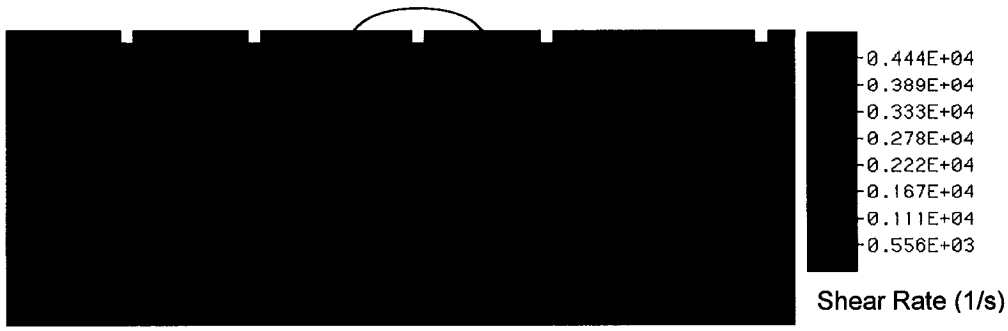

Figure 23-(a): Shear rate distribution in the blood at peak forward flow

Figure 23-(b): Zoomed-in view of the shear rate distribution in the near strut region encircled in figure (a)

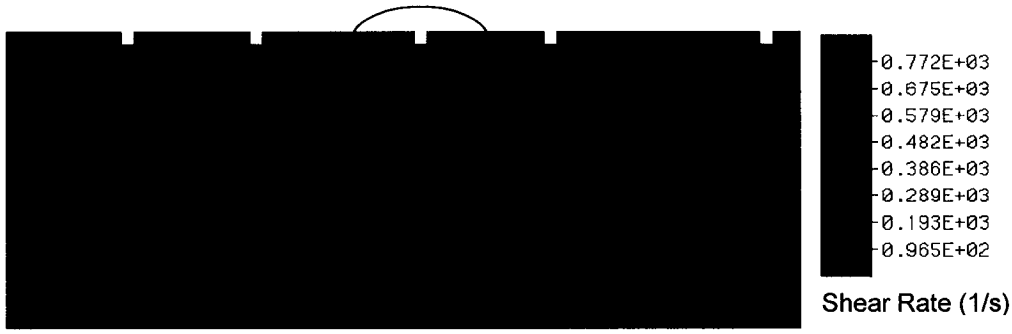

Figure 23-(c): Shear rate distribution in the blood at peak backward flow

Figure 23-(d): Zoomed-in view of the shear rate distribution in the near strut region encircled in figure (c)

Figure 23: Shear rate distribution in the blood on the section defined in Figure 4

7. Wall Shear Stress Fluctuations

Wall shear rate was plotted with respect to time for two points on the artery wall: One in the center of the positive hexagon cell and a second one within the same cell but 55 μm downstream of the strut (Figure 24). The two shear rate plots show that, throughout the pulse period, the temporal wall shear gradient is higher for the point that is distant from the struts, which also exhibits higher shear rate values. We can also notice that the difference between the two plots varies with time and is highest at peak forward flow. This variation is an indication of how the wall shear stress gradient (WSSG) changes with time.

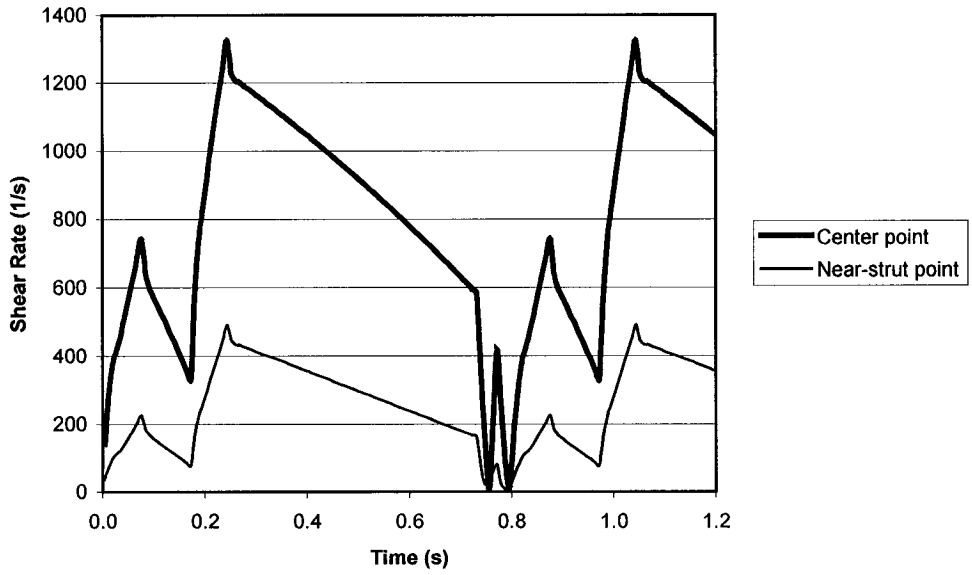

Figure 24: Shear rate fluctuation with respect to time for two points on artery wall

8. Comparison with Healthy and Stenosed Arteries

To evaluate the changes that the deployment of a stent introduces into the hymodynamics of the artery we compared the values of maximum shear rate between the healthy, the stenosed, and the stented models as shown in Table 4.

Model	Peak Forward Flow	Peak Backward Flow
Healthy Artery	2.07×10^3	6.19×10^2
Stenosed Artery	1.98×10^4	1.14×10^3
Stented Artery (Wall)	1.80×10^3	3.76×10^2
Stented Artery (Struts)	5.91×10^3	8.62×10^2

Table 4: Maximum shear rate in (1/s) for the different models

Chapter 7: Analysis

1. Mesh Resolution Requirements

To assess the suitability of the mesh adopted for the simulations, we used a series of meshes with different mesh densities, especially at the near wall region, to investigate mesh-independence. Our results are in accordance with the findings of Prakash and Ethier (2001) [70] in their study of the impact of mesh characteristics on the velocity and wall shear stress patterns in a human right coronary artery. In particular, our results support the fact that mesh-independent velocity fields were easier to obtain compared to the wall shear stress fields. However, in their study, it was not possible to obtain a trend towards mesh-independence using a conventional mesh series. They were only able to obtain it through adaptive mesh. On the other hand, our mesh series showed a tendency towards mesh-independence without the use of adaptive mesh. The main reason behind this difference may be the fact that in their model tetrahedral elements were used to form the grid, while in our mesh was made of mapped hexahedral elements.

In addition, our results show that for the study of the hemodynamics in stented arteries, special attention has to be paid to the mesh at the tip of the struts. It required higher mesh resolution to obtain mesh-independence for the shear stress field at the tip of the struts compared to other areas like the artery wall for example. This is mainly due to the fact that the flow changes rapidly both in direction and magnitude at the corners of the struts. This observation is supported by the PIV

study of Benard et al (2003)[60] in which they found the highest values of shear stress to be close to the stent struts.

2. Secondary Flow Analysis

One of the main advantages of 3D modeling is the capacity to study the out-of-plane flow characteristics and their possible effects on the development of the disease.

The results of the present investigation demonstrate the existence of significant secondary flow in the near-wall region of the stented segment of the artery. This result is supported by the study of LaDisa et al (2003) [64] in which they found the Palmaz-Schatz stent to produce significant out-of-plane motion of the secondary component of the velocity vector. Particularly interesting is the fact that secondary flow is more pronounced in the areas following struts that are perpendicular to the main flow direction, but almost disappears as we move away from these struts to the middle of the inter-strut zone. This observation can ultimately be used to explain the results of an endothelial cell regrowth study presented by Frank et al(2002) [71]. In this study, porcine aortic endothelial cells are seeded inside a flat plate stented flow chamber to measure their regrowth using video images. In a video image taken after 96 hours of exposing the cells to pulsatile flow (Figure 25) the cells morphology shows greater alignment parallel to the bars that are perpendicular to the main flow direction. In addition, cells in the central region of the inter-strut zone show greater alignment with the flow direction. This difference in cell alignment may be explained in light of the patterns of secondary flow described in the present study.

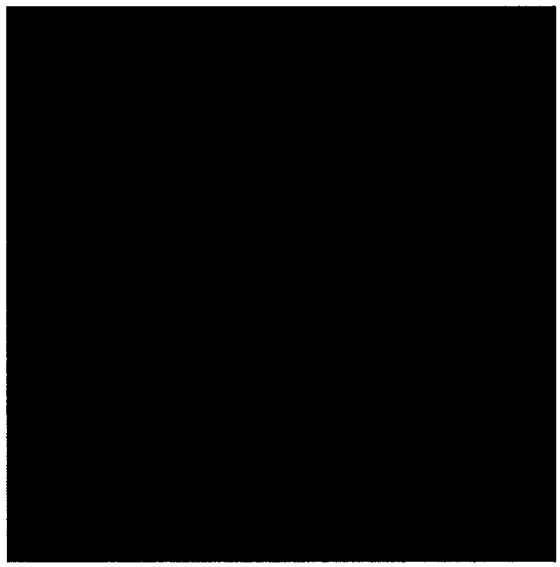

Figure 25: Video image of EC regrowth from experimental flow studies (flow is left to right) Reproduced with permission from [71].

Another important result in the study of secondary flow is the observation that the effect of the stent struts in generating out-of-plane motion velocity component does not propagate to the center of the artery. Rather, in all the sections studied, secondary flow was limited to an annulus in the near wall region. This result implies that in-vitro experiments in flat stented flow chambers can be used to study the flow patterns in a stented segment of an artery.

3. Shear Rate Distribution

The effect of shear stress distribution on neointimal hyperplasia and hence on the development of ISR, has been well documented by a number of preceding studies [72-75]. In particular, it has been shown that the augmentation of WSS inhibits

neointimal hyperplasia while regions of low and oscillatory shear stress have been associated with intimal thickening.

The results of the present study show significant alterations to shear stress distribution on the artery wall and in the near wall region introduced by the presence of the stent. Similar distribution, with high shear values on the tip of the struts and low shear around the struts, have been reported by experimental studies such as Benard et al (2001) [60] and by CFD studies such as LaDisa et al (2005) [65]. Of particular interest is the fact that the closed cells exhibit higher shear values compared to the span area between the strut rings that include only two connecting struts around the circumference. This observation could contribute to the explanation of the findings of the study by Ikari et al (1995) [76] in which they observed higher luminal loss at the articulation of a Palmaz-Schatz stent compared to other segments of the stent after 6 months of stent implantation (Figure 26).

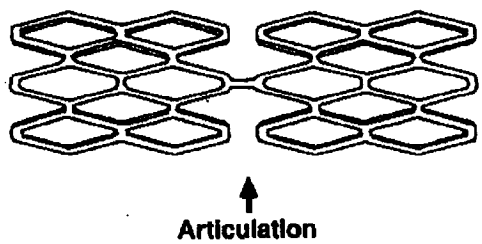

Figure 26: Palmaz-Schatz stent articulation

However, they attribute this difference in intimal response between the different stent segments to more severe injury caused by the articulation, and to delayed vessel remodeling from lack of mechanical support. Nevertheless, the results of the current study show that the difference in the WSS distribution between the different stent segments may be an important factor in explaining their results. Another aspect of

the WSS distribution that can also explain their findings is the fact that zones of low shear stress seem to be larger at the junction points which are similar to the articulation anchors in the Palmaz-Schatz stent.

Another aspect of the shear stress distribution that can be an initiating factor for the development of ISR is the high shear values observed at the tip of the struts. In fact, Olgun et al (2004)[77] have stated that after the destruction of the red blood cells released hemoglobin can contribute to the development of atherosclerosis. Similarly, the high shear values observed at the tip of the struts can lead to the destruction of the red blood cells, especially the fragile and old ones, and lead to the development of the ISR. If this hypothesis is validated it will implicate that the use of streamlined struts that do not have sharp corners may help in decreasing the rate of restenosis.

4. Wall Shear Stress Fluctuations

In his book "The Fluid Mechanics of Large Blood Vessels", Pedley argued that the unsteady components of the wall shear stress (WSS) are likely to be at least as important as the mean shear in determining the role of shear stress in the physiological changes in arterial tissues [78]. Many studies that followed have established a relation between the temporal oscillations in WSS and the development of restenosis [79]. The present results show that the highest WSS fluctuations occur in the middle of the span between the stent struts. They also show significant variation of the WSS gradient in the inter-strut zone. This variation can result in an amplification of the morphological and functional changes to the endothelium by

endothelial cells division due to the variation of the conflicting forces applied on adjacent cells because of the special gradient of WSS [80].

5. Limitations and Future Research

The results of the present study should be interpreted within the constraints of certain limitations. First, the simulations do not take into consideration the non-Newtonian effects of the blood. While blood behaves generally like a Newtonian fluid at high shear rates, the non-Newtonian properties may affect the blood flow patterns and shear stress results at zones or times of low shear rate. In addition, our geometric model is based on a representation of a straight blood vessel, while in a number of cases stents are placed in curved or branching vessels. The vessel curvature can have significant effect on the skewness of the velocity profile and the general behaviour of the flow in the stented segment. Another geometric limitation of the present study is the fact that we don't take the composition of the atherosclerotic plaque into consideration. The composition of the plaque can significantly affect the inner geometry of the lumen and result in asymmetric stent expansion, which was shown by Schulz et al (2000) [81] to correlate with the development of ISR. Furthermore, this study does not take into consideration vessel compliance; rather it considers the artery as a rigid wall boundary. Although a number of studies have reported very low compliance in the stented segment of the artery [58, 62], the compliance at the distal and proximal ends of the stent may still have significant effect on the local hemodynamics. Until now, to the best of the

author's knowledge, no study has reported the use of fluid structure interaction for the investigation of blood flow patterns or vessel wall behaviour in a stented artery.

Conclusion

The present study presents a characterization of the local hemodynamics in a stented coronary artery using time-dependent 3D CFD models. This characterization is meant to improve our understanding of the mechanisms by which the variations in blood flow patterns and shear stress distribution in the stented segment of the artery may affect the development of ISR. The present results support several findings of previous studies and can be used as explanations for certain phenomena observed after stent implantation. In particular, the results of this study support the hypothesis that the local hemodynamics affect endothelial cell regrowth and platlet adhesion, and eventually noeintimal hyperplasia. These results can be taken into consideration in future stent designs to improve their rate of success by introducing geometric changes that make the local hemodynamics favorable to inhibiting the development of ISR.

References

1. Witztum, J.L., *Thematic reviews on the pathogenesis of atherosclerosis.* J Lipid Res, 2004. **45**(6): p. 991-2.
2. *The World Health Report 2004*, World Health Organization (WHO). p. Statistical Annex - Annex table 2.
3. Noll, G., *Pathogenesis of atherosclerosis: a possible relation to infection.* Atherosclerosis, 1998. **140 Suppl 1**: p. S3-9.
4. Ross, R., *The pathogenesis of atherosclerosis: a perspective for the 1990s.* Nature, 1993. **362**(6423): p. 801-9.
5. Steinberg, D., *Thematic review series: The Pathogenesis of Atherosclerosis. An interpretive history of the cholesterol controversy: part I.* J Lipid Res, 2004. **45**(9): p. 1583-93.
6. Fruchart, J.C., et al., *New risk factors for atherosclerosis and patient risk assessment.* Circulation, 2004. **109**(23 Suppl 1): p. III15-9.
7. Misra, A., *Risk factors for atherosclerosis in young individuals.* J Cardiovasc Risk, 2000. **7**(3): p. 215-29.
8. Kullo, I.J., G.T. Gau, and A.J. Tajik, *Novel risk factors for atherosclerosis.* Mayo Clin Proc, 2000. **75**(4): p. 369-80.
9. Capron, L., *[Pathogenesis of atherosclerosis: an update on the three main theories].* Ann Cardiol Angeiol (Paris), 1989. **38**(10): p. 631-4.

10. Fuster, V., R. Ross, and E.J. Topol, *Atherosclerosis and coronary artery disease*. 1996, Philadelphia: Lippincott-Raven. 2 v. (xxv, 1661, 42).

11. Glasser, S.P., A.P. Selwyn, and P. Ganz, *Atherosclerosis: risk factors and the vascular endothelium.* Am Heart J, 1996. **131**(2): p. 379-84.

12. Franklin, B.A. and J.K. Kahn, *Delayed progression or regression of coronary atherosclerosis with intensive risk factor modification. Effects of diet, drugs, and exercise.* Sports Med, 1996. **22**(5): p. 306-20.

13. Paoletti, R., F. Bruno, and S. Colli, *Atherosclerosis and thrombosis. Old and new drugs.* Arch Gerontol Geriatr, 1995. **20**(1): p. 43-8.

14. Chobanian, A.V., *Can antihypertensive drugs reduce atherosclerosis and its clinical complications?* Am J Hypertens, 1994. 7(10 Pt 2): p. 119S-125S.

15. MacGillivray, T.E. and G.J. Vlahakes, *Patency and the pump--the risks and benefits of off-pump CABG.* N Engl J Med, 2004. **350**(1): p. 3-4.

16. Arjomand, H., et al., *Percutaneous coronary intervention: historical perspectives, current status, and future directions.* Am Heart J, 2003. **146**(5): p. 787-96.

17. Morimoto, S., et al., *Mechanism of luminal enlargement in PTCA and restenosis: a histopathological study of necropsied coronary arteries collected from various centers in Japan.* Jpn Circ J, 1987. **51**(9): p. 1101-15.

18. Danchin, N. and P. Urban, *PTCA versus CABG: a different interpretation of the results of randomised trials comparing both treatments.* Heart, 1999. **82**(4): p. 413-4.

19. Goldsmith, M.F., *Once again, CABG vs PTCA--trial results today.* Jama, 1994. **271**(4): p. 257.

20. Eberli, F.R. and B. Meier, *Coronary bypass surgery vs coronary angioplasty: a look to the past for new insights into the future.* Eur Heart J, 2002. **23**(7): p. 511-4.

21. Serruys, P.W., et al., *A comparison of balloon-expandable-stent implantation with balloon angioplasty in patients with coronary artery disease. Benestent Study Group.* N Engl J Med, 1994. **331**(8): p. 489-95.

22. Betriu, A., et al., *Randomized comparison of coronary stent implantation and balloon angioplasty in the treatment of de novo coronary artery lesions (START): a four-year follow-up.* J Am Coll Cardiol, 1999. **34**(5): p. 1498-506.

23. Alfonso, F., et al., *A randomized comparison of repeat stenting with balloon angioplasty in patients with in-stent restenosis.* J Am Coll Cardiol, 2003. **42**(5): p. 796-805.

24. Karthikeyan, G. and B. Bhargava, *Prevention of restenosis after coronary angioplasty.* Curr Opin Cardiol, 2004. **19**(5): p. 500-9.

25. Cwikiel, W., *Restenosis after balloon angioplasty and/or stent insertion - origin and prevention.* Acta Radiol, 2002. **43**(5): p. 442-54.

26. Kereiakes, D., et al., *Usefulness of stent length in predicting in-stent restenosis (the MULTI-LINK stent trials).* Am J Cardiol, 2000. **86**(3): p. 336-41.

27. Foley, D.P., R. Melkert, and P.W. Serruys, *Influence of coronary vessel size on renarrowing process and late angiographic outcome after successful balloon angioplasty.* Circulation, 1994. **90**(3): p. 1239-51.

28. Hirshfeld, J.W., Jr., et al., *Restenosis after coronary angioplasty: a multivariate statistical model to relate lesion and procedure variables to restenosis. The M-HEART Investigators.* J Am Coll Cardiol, 1991. **18**(3): p. 647-56.

29. Sobel, B.E., *Acceleration of restenosis by diabetes: pathogenetic implications.* Circulation, 2001. **103**(9): p. 1185-7.

30. Rakugi, H., et al., *Potential importance of tissue angiotensin-converting enzyme inhibition in preventing neointima formation.* Circulation, 1994. **90**(1): p. 449-55.

31. Kranzhofer, R., et al., *Suppression of neointimal thickening and smooth muscle cell proliferation after arterial injury in the rat by inhibitors of Na(+)-H+ exchange.* Circ Res, 1993. **73**(2): p. 264-8.

32. Cavusoglu, E., et al., *Current status of rotational atherectomy.* Catheter Cardiovasc Interv, 2004. **62**(4): p. 485-98.

33. Holmes, D.R., Jr., *In-stent restenosis.* Rev Cardiovasc Med, 2001. **2**(3): p. 115-9.

34. Kandzari, D.E., J.E. Tcheng, and J.P. Zidar, *Coronary artery stents: evaluating new designs for contemporary percutaneous intervention.* Catheter Cardiovasc Interv, 2002. **56**(4): p. 562-76.

35. Serruys, P.W. and B. Rensing, *Handbook of coronary stents*. 4th ed. 2002, London: Martin Dunitz. xiii, 366 p.

36. Stoeckel, D., C. Bonsignore, and S. Duda, *A survey of stent designs.* Minimally InvasiveTherapy & Allied Technology, 2002. **11**(4): p. 137-147.

37. Miketic, S., J. Carlsson, and U. Tebbe, *Randomized comparison of J&J Crown stent versus NIR stent after routine coronary angioplasty.* Am Heart J, 2001. **142**(5): p. E8.

38. Nakatani, M., et al., *Mechanisms of restenosis after coronary intervention: difference between plain old balloon angioplasty and stenting.* Cardiovasc Pathol, 2003. **12**(1): p. 40-8.

39. Hoffmann, R., et al., *Patterns and mechanisms of in-stent restenosis. A serial intravascular ultrasound study.* Circulation, 1996. **94**(6): p. 1247-54.

40. Indolfi, C., et al., *Molecular mechanisms of in-stent restenosis and approach to therapy with eluting stents.* Trends Cardiovasc Med, 2003. **13**(4): p. 142-8.

41. Nakatogawa, T., et al., *Impact of peri-stent remodeling on in-stent neointimal proliferation in acute myocardial infarction.* Am J Cardiol, 2004. **94**(6): p. 769-71.

42. Berry, J.L., et al., *Hemodynamics and wall mechanics of a compliance matching stent: in vitro and in vivo analysis.* J Vasc Interv Radiol, 2002. **13**(1): p. 97-105.

43. Friedman, M.H., et al., *Correlation between intimal thickness and fluid shear in human arteries.* Atherosclerosis, 1981. **39**(3): p. 425-36.

44. Gnasso, A., et al., *Association between intima-media thickness and wall shear stress in common carotid arteries in healthy male subjects.* Circulation, 1996. **94**(12): p. 3257-62.

45. Ku, D.N., et al., *Pulsatile flow and atherosclerosis in the human carotid bifurcation. Positive correlation between plaque location and low oscillating shear stress.* Arteriosclerosis, 1985. **5**(3): p. 293-302.

46. Moore, J.E., Jr., et al., *Pulsatile flow visualization in the abdominal aorta under differing physiologic conditions: implications for increased susceptibility to atherosclerosis.* J Biomech Eng, 1992. **114**(3): p. 391-7.

47. He, X. and D.N. Ku, *Pulsatile flow in the human left coronary artery bifurcation: average conditions.* J Biomech Eng, 1996. **118**(1): p. 74-82.

48. Tominaga, R., et al., *Effects of stent design and serum cholesterol level on the restenosis rate in atherosclerotic rabbits.* Am Heart J, 1993. **126**(5): p. 1049-58.

49. Rogers, C. and E.R. Edelman, *Endovascular stent design dictates experimental restenosis and thrombosis.* Circulation, 1995. **91**(12): p. 2995-3001.

50. Hoffmann, R., et al., *Stent design related neointimal tissue proliferation in human coronary arteries; an intravascular ultrasound study.* Eur Heart J, 2001. **22**(21): p. 2007-14.

51. Kastrati, A., et al., *Restenosis after coronary placement of various stent types.* Am J Cardiol, 2001. **87**(1): p. 34-9.

52. Cheng, G.C., et al., *Mechanical strain tightly controls fibroblast growth factor-2 release from cultured human vascular smooth muscle cells.* Circ Res, 1997. **80**(1): p. 28-36.

53. Schwartz, R.S., et al., *Restenosis and the proportional neointimal response to coronary artery injury: results in a porcine model.* J Am Coll Cardiol, 1992. **19**(2): p. 267-74.

54. Garasic, J.M., et al., *Stent and artery geometry determine intimal thickening independent of arterial injury.* Circulation, 2000. **101**(7): p. 812-8.

55. Peacock, J., et al., *Flow instabilities induced by coronary artery stents: assessment with an in vitro pulse duplicator.* J Biomech, 1995. **28**(1): p. 17-26.

56. Wakhloo, A.K., et al., *Self-expanding nitinol stents in canine vertebral arteries: hemodynamics and tissue response.* AJNR Am J Neuroradiol, 1995. **16**(5): p. 1043-51.

57. Lee, B.K., et al., *Hemodynamic analysis of coronary circulation in angulated coronary stenosis following stenting.* Yonsei Med J, 2002. **43**(5): p. 590-600.

58. LaDisa, J.F., Jr., et al., *Stent implantation alters coronary artery hemodynamics and wall shear stress during maximal vasodilation.* J Appl Physiol, 2002. **93**(6): p. 1939-46.

59. Berry, J.L., et al., *In Vitro Flow Visualization in Stented Arterial Segments.* Journal of Vascular Investigation, 1997. **3**(2): p. 63-68.

60. Benard, N., et al., *Experimental study of laminar blood flow through an artery treated by a stent implantation: characterisation of intra-stent wall shear stress.* J Biomech, 2003. **36**(7): p. 991-8.

61. Henry, F., *Flow in a stented artery*, in *Intra and Extra Corporeal Cardiovascular Fluid Dynamics*, K.P. P Vendonck, Editor. 2000, WIT Press: Southhampton, UK. p. 333-64.

62. Berry, J.L., et al., *Experimental and computational flow evaluation of coronary stents.* Ann Biomed Eng, 2000. **28**(4): p. 386-98.

63. Schachter, L.G., Barakat,A. I. *Computational Study of Arterial Flow Disturbance Induced by Intravascular Stents.* in *ASME Summer Bioengineering Conference*. 2001. Snowbird, UT. New York.

64. LaDisa, J.F., Jr., et al., *Three-dimensional computational fluid dynamics modeling of alterations in coronary wall shear stress produced by stent implantation.* Ann Biomed Eng, 2003. **31**(8): p. 972-80.

65. Ladisa, J.F., Jr., et al., *Circumferential vascular deformation after stent implantation alters wall shear stress evaluated with time-dependent 3D computational fluid dynamics models.* J Appl Physiol, 2005. **98**(3): p. 947-57.

66. Fung, Y.C., *Biomechanics : mechanical properties of living tissues.* 2nd ed. 1993, New York: Springer-Verlag. xviii, 568.

67. Feldman, C.L., et al., *Determination of in vivo velocity and endothelial shear stress patterns with phasic flow in human coronary arteries: a methodology to predict progression of coronary atherosclerosis.* Am Heart J, 2002. **143**(6): p. 931-9.

68. O'Callaghan, S., M. Walsh, and T. McGloughlin. *Comparison of Finite Volume, Finite Element and Theoretical Predictions of Blood Flow Through an Idealised Femoral Artery.* in *2003 Summer Bioengineering Conference*. 2003. Key Biscayne, Florida.

69. Tang, T.D., D.P Giddens, C.K. Zarins, S. Glagov, *Velocity Profile and Wall Shear Measurements in a Model Human Coronary Artery.* Advances in Bioengineerings, 1990: p. 261-263.

70. Prakash, S. and C.R. Ethier, *Requirements for mesh resolution in 3D computational hemodynamics.* J Biomech Eng, 2001. **123**(2): p. 134-44.

71. Frank, A.O., P.W. Walsh, and J.E. Moore, Jr., *Computational fluid dynamics and stent design.* Artif Organs, 2002. **26**(7): p. 614-21.

72. Wentzel, J.J., et al., *Shear stress, vascular remodeling and neointimal formation.* J Biomech, 2003. **36**(5): p. 681-8.

73. Edelman, E.R. and C. Rogers, *Pathobiologic responses to stenting.* Am J Cardiol, 1998. **81**(7A): p. 4E-6E.

74. Stone, P.H., et al., *Effect of endothelial shear stress on the progression of coronary artery disease, vascular remodeling, and in-stent restenosis in humans: in vivo 6-month follow-up study.* Circulation, 2003. **108**(4): p. 438-44.

75. Carlier, S.G., et al., *Augmentation of wall shear stress inhibits neointimal hyperplasia after stent implantation: inhibition through reduction of inflammation?* Circulation, 2003. **107**(21): p. 2741-6.

76. Ikari, Y., et al., *Luminal loss and site of restenosis after Palmaz-Schatz coronary stent implantation.* Am J Cardiol, 1995. **76**(3): p. 117-20.

77. Olgun, A., S. Akman, and M.K. Erbil, *The role of RBC destruction in vascular regions with high turbulence on atherosclerosis.* Med Hypotheses, 2004. **63**(2): p. 283-4.

78. Pedley, T.J., *The fluid mechanics of large blood vessels*. 1980, Cambridge ; New York: Cambridge University Press. xv, 446.

79. Kleinstreuer, C., et al., *Hemodynamic parameters and early intimal thickening in branching blood vessels.* Crit Rev Biomed Eng, 2001. **29**(1): p. 1-64.

80. DePaola, N., et al., *Vascular endothelium responds to fluid shear stress gradients.* Arterioscler Thromb, 1992. **12**(11): p. 1254-7.

81. Schulz, C., et al., *Coronary stent symmetry and vascular injury determine experimental restenosis.* Heart, 2000. **83**(4): p. 462-7.

Appendix A: FIDAP input file

```
/
/  INPUT FILE
/
/ ***  FICONV Conversion Commands ***
/ ***  Remove / to uncomment as needed
/
FICONV(NEUTRAL,NORESULTS,INPUT)
INPUT(FILE= "periodic3.FDNEUT")
END
/  *** of FICONV Conversion Commands
/
TITLE
3D-Cylindrical-Pulsatile
CONFIG(FIDAPMEM=200000000,FISOLVMEM=0, COMPRESS, SHOW)
/
/ ***  FIPREP  Commands ***
/
FIPREP
 PROB (3-D, INCO, TRAN, LAMI, NONL, NEWT, MOME, ISOT, FIXE, NOST, NORE, SING)
 EXEC (NEWJ)
 SOLU (SEGR = 200, VELC = 0.100000000000E-02, SCHANGE = 0, CR, CGS, NCGC = 1E-6,
         SCGC = 1E-6, ACCF = 0.0)
 TIME (BACK, NSTE = 600, TSTA = 0.000000000000E+00, DT = 0.002, FIXE)
 DATA (CONT)
 PRIN (NONE, BOUN)
 TMFU (SET = 1, NPOI = 13)
  0.0000000000E+00,  0.0000000000E+00,  0.0800000000E+00,  0.4700000000,
  0.1760000000E+00,  0.2400000000E+00,  0.248000000,  0.1000000000E+01,
  0.736000000,  0.4100000000E+00,  0.776,-0.07,   0.8,0, 0.88,0.47,  0.976,0.24,  1.048,1,
  1.536,0.41,  1.576,-0.07,  1.6,0
/
/Entities
/
 ENTI (NAME = "lumen", FLUI, MDEN = 1, MVIS = 1)
 ENTI (NAME = "wall", PLOT)
 ENTI (NAME = "struts", PLOT)
 ENTI (NAME = "strside", PLOT)
 ENTI (NAME = "inlet", PLOT)
 ENTI (NAME = "outlet", PLOT)
 ENTI (NAME = "sym1", SLIP)
 ENTI (NAME = "sym2", SLIP)
 ENTI (NAME = "center", SLIP)
 ENTI (NAME = "sidesin", PLOT)
 ENTI (NAME = "sideout", PLOT)
/
/Properties
/
 DENS (SET = 1, CONS = 0.173200000000E-10)
 VISC (SET = 1, CONS = 0.889000000000E-05)
/
/Boundary Conditions
```

```
/
 BCPE (VELO, UN3, ENTI, REFE = "sym1", PERI = "sym2", EXCL, R1NO = 269,
     R2NO = 2188, P1NO = 356, P2NO = 1679)
 BCNO (VELO, ENTI = "wall", ZERO, X, Y, Z)
 BCNO (VELO, ENTI = "struts", ZERO, X, Y, Z)
 BCNO (VELO, ENTI = "strside", ZERO, X, Y, Z)
 BCNO (UN3, ENTI = "center", ZERO)
 BCNO (UX, ENTI = "inlet", ZERO)
 BCNO (UY, ENTI = "inlet", ZERO)
 /Re_peak_sys = 640
 BCNO (UZ, ENTI = "inlet", POLY = 1, CURV=1, SYST = 1, CYLI)
  547584, -1.522,  0.2000000000E+01,  0.0000000000E+00,
  0.0000000000E+00
/ BC's for inlet edges
 BCSYS (SET=3, NORMAL)
 0 0 1
 BCNO (COOR, CONS=3, ENTITY="sidesin")
 BCNO (VELO, FREE, ENTITY = "sidesin")
 BCNO (UN3, ENTI = "sidesin", POLY = 1, CURV=1, SYST = 1, CYLI)
  547584, -1.522,  0.2000000000E+01,  0.0000000000E+00,
  0.0000000000E+00
 BCNO (UT1, ENTI = "sidesin", ZERO)
 BCNO (UT2, ENTI = "sidesin", ZERO)
/
/BC for outlet edge
BCSYS (SET=4, NORMAL)
 1 1 0
 BCNO (COOR, CONS=4, ENTITY="sideout")
 BCNO (VELO, FREE, ENTITY = "sideout")
 BCNO (UN3, ENTI = "sideout", ZERO)
/
 BCNO (PRES, ENTI = "outlet", zero)
 POSTPROCESS(NBLOCKS=1)
 1 600 2

END
/  *** of FIPREP Commands
 CREATE(FISOLV)
/RUN (FISOLV, FOREGROUND)
```

Appendix B: Iterative methods used with the

1. Conjugate Residual (CR) Method

This method is used for the solution of symmetric equation system associated with the pressure solution and its algorithm is given by:

Consider the system of N linear equations: $\mathbf{A x = b}$

where **A** is a symmetric matrix. Given an initial guess x_o, a sequence $\{x_n\}$ of approximations to the solution **x** is generated as follows:

1. Choose x_o
2. Set $r_o = b - A x_o$
3. Set $p_o = r_o$
4. For i =0,1,2, . . . until convergence do:

$$a_i = \frac{(r_i, r_i)}{(p_i, Ap_i)}$$

$a_i = (r_i , r_i)/(p_i , A p_i)$

$x_{i+1} = x_i + a_i p_i$

$r_{i+1} = r_i - a_i A p_i$

$b_i = (r_{i+1} , r_{i+1})/ (r_i , r_i)$

$p_{i+1} = r_{i+1} + b_i p_i$

2. Conjugate Gradient Squared (CGS) Method

This method is used for solving the non-symmetric, non-positive real systems of equations and it can be described as follows:

1. Choose x_0
2. Set $r_0 = b - \mathbf{A}x_0$
3. Set $g_0 = u_0 = r_0^* = r_0$
4. For i =0,1,2, . . . until convergence do:

   $$p_{i+1} = u_i - a_i \mathbf{A} g_i$$

   $$x_{i+1} - x_i + a_i(u_i + p_{i+1})$$

   $$r_{i+1} = r_i - a_i \mathbf{A}(u_i + p_{i+1})$$

   $$u_{i+1} = r_{i+1} + b_i p_{i+1}$$

   $$g_{i+1} = u_{i+1} + b_i(b_i g_i + p_{i+1})$$

   where

   $$a_i = (r_0^*, r_i) / (r_0^*, \mathbf{A}g_i)$$

   $$b_i = (r_0^*, r_{i+1}) / (r_0^*, r_i)$$